Diet, cellular, and systemic homeostasis control the cycling of potassium stable isotopes in endothermic vertebrates

T Tacail, J Lewis, M Clauss, C Coath, R Evershed, E Albalat, T Elliott, T Tütken

Diet, cellular, and systemic homeostasis control the cycling of potassium stable isotopes in endothermic vertebrates

T. Tacail [1,2,*], J. Lewis [2], M. Clauss [3], C. D. Coath [2], R. Evershed [4], E. Albalat [5], T. R. Elliott [2] and T. Tütken [1]

[1]Institute of Geosciences, Johannes Gutenberg University, J.-J.-Becher-Weg 21, D-55128, Mainz, Germany, [2]School of Earth Sciences, University of Bristol, Bristol, UK, [3]Clinic for Zoo Animals, Exotic Pets and Wildlife, Vetsuisse Faculty, University of Zurich, Switzerland, [4]Organic Geochemistry Unit, School of Chemistry, University of Bristol, UK and [5]ENS de LYON, Universite Claude Bernard Lyon1, LGL-TPE, CNRS UMR 5276, Lyon, France
*__Correspondence__: Institute of Geosciences, Johannes Gutenberg University, J.-J.-Becher-Weg 21, D-55128, Mainz, Germany. E-mail: theo.tacail@protonmail.com

Abstract

The naturally occurring stable isotopes of potassium ($^{41}K/^{39}K$, expressed as $\delta^{41}K$) have the potential to make significant contributions to vertebrate and human biology. The utility of K stable isotopes is, however, conditioned by the understanding of the dietary and biological factors controlling natural variability of $\delta^{41}K$. This paper reports a systematic study of K isotopes in extant terrestrial endothermic vertebrates. $\delta^{41}K$ has been measured in 158 samples of tissues, biofluids, and excreta from 40 individuals of four vertebrate species (rat, guinea pig, pig and quail) reared in two controlled feeding experiments. We show that biological processing of K by endothermic vertebrates produces remarkable intra-organism $\delta^{41}K$ variations of ca. 1.6‰. Dietary $\delta^{41}K$ is the primary control of interindividual variability and $\delta^{41}K$ of bodily K is +0.5–0.6‰ higher than diet. Such a trophic isotope effect is expected to propagate throughout trophic chains, opening promising use for reconstructing dietary behaviors in vertebrate ecosystems. In individuals, cellular $\delta^{41}K$ is related to the intensity of K cycling and effectors of K homeostasis, including plasma membrane permeability and electrical potential. Renal and intestinal transepithelial transports also control fractionation of K isotopes. Using a box-modeling approach, we establish a first model of K isotope homeostasis. We predict a strong sensitivity of $\delta^{41}K$ to variations of intracellular and renal K cycling in normal and pathological contexts. Thus, K isotopes constitute a promising tool for the study of K dyshomeostasis.

Keywords: bones, diet, homeostasis, K isotopes, soft tissues, stable isotope metallomics

Graphical abstract

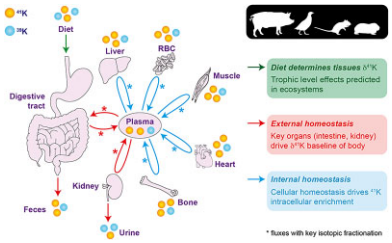

The natural abundances of potassium stable isotopes in endothermic vertebrates are controlled by diet and by the cellular and systemic cycling of potassium.

Introduction

Over the last decade, the study of the naturally occurring stable isotopes of essential metals in vertebrates (e.g. Ca, Mg, Fe, Zn, Cu) has opened novel avenues of research contributing new results in the study of the biology of present and past vertebrates. These fields of research have helped to determine the dietary sources of these metals, as researched in "isotope paleobiology."[1–5] Such approaches have also helped detect, with increasingly fine detail, metabolic imbalances in health or disease, which may otherwise remain unseen when focusing on elemental quantification of metals alone, as studied in "isotope metallomics."[3,6–8] This utility of metal stable isotopes in such research primarily relies on the understanding of the underlying metabolic factors controlling the distributions of metal isotopes in organisms, both at steady state and in response to normal or pathologic perturbations. In this aspect, the stable isotopes of potassium (K) for such applications remain unexplored.

Potassium is a ubiquitous and essential alkali metal found in all vertebrates. It constitutes the most abundant inorganic ion (K^+) of the intracellular fluids (ICF) and plays a vital role in systemic functions, related to processes such as cell signaling, muscle contraction, and energy metabolismwith.[9–11] Potassium has two naturally occurring and stable isotopes,^{39}K (93.2581%) and ^{41}K (6.7302%), as well as a rare radioactive isotope (^{40}K, 0.0117%).[12] This isotopic configuration has made the precise determination of K stable isotope ratios ($^{41}K/^{39}K$) problematic by thermal ionization

mass spectrometry.[13,14] Furthermore, the measurement of the $^{41}K/^{39}K$ with conventional multi-collection inductively coupled-plasma mass spectrometry (MC-ICP-MS) is severely hampered by major interferences due to the Ar species derived from inductively coupled Ar plasma. Only recently, technological and methodological innovations such as cold plasma,[15,16] enhanced high mass resolution,[17] or collision-cell MC-ICP-MS,[18–21] have enabled the precise and accurate measurement of K stable isotope compositions. These methods have allowed the initial characterization of reference materials and exploration of natural systems in both geological and biological settings.[17,20,22–36]

Exploratory datasets and reference materials covering a wide array of vegetal and animal samples in marine and terrestrial settings show that the biologically induced variability of $^{41}K/^{39}K$ ratios is sizeable (in the order of 2–3‰) and exceeds the variability observed in most igneous and sedimentary rocks (e.g. Hobin *et al.*,[17] Wang *et al.*,[29] Moynier *et al.*[30]). The biological processing of K therefore clearly induces major isotope fractionations. The systematics and controls of these biological isotope effects were notably explored in terrestrial plant tissues, including rice, wheat and soybean grown in controlled conditions[32] as well as trees and grass samples from forest and grassland ecosystems.[37] Higgins *et al.*[31] recently published reporting cellular and transepithelial controls of K isotopes variability in green algae, teleost fishes, and rats. However, the K isotope homeostasis of vertebrates remains to be documented and characterized in a systematic and dedicated research approach. To estimate the relevance of K stable isotopes for the study of vertebrate biology and develop their use in isotope paleobiology and metallomics, it is therefore necessary to identify the main factors controlling these distributions.

Potassium homeostasis in endothermic vertebrates

Potassium in vertebrates is characterized by heterogeneous and physiologically controlled distributions at all scales, from single cells to the organs, reflecting the key functions to which K contributes. The vast majority of K in vertebrates is found in ICF (≈98% of total body K), the remainder being mainly transported as free cations in the extracellular fluids (ECF), such as blood plasma.[10,38,39] Most of body K is stored in muscle cells (70–75%), while liver, red blood cells (RBC), bone, skin, and brain host the majority of the rest of the K budget.[10,38–40]

At the scale of the cell, K distribution is directly related to cellular and systemic functions. The vertebrate cell actively maintains a steep K transmembrane concentration gradient, with ICF K concentrations being roughly one order of magnitude higher than in ECF (ca. 140 mM vs. ca. 10 mM, respectively).[9] This gradient is the opposite of what is observed for sodium cations (Na^+), which have lower concentrations in ICF than in ECF.[9,38,41] The heterogeneous distributions of K and Na primarily result from the continuous action of the Na/K-ATPase integral membrane protein (NKA). The NKA sends $2K^+$ to the ICF while pumping $3Na^+$ to the ECF at the cost of one ATP molecule.[9] This highly conserved protein is found in all animal cells and its baseline activity accounts for a substantial fraction of the total organism basal energy consumption (25–30% of the total organism ATP use in mammals).[9,42,43] The K influx to the ICF is continuously balanced by a K efflux, owing to the presence of K-specific channels of the two-pore domain family.[9] As a result of the combination of these K chemical gradients and K-specific outward permeability, the K cell homeostasis is primarily responsible for the electrochemical gradients of cells at rest, also referred to as resting membrane potentials (RMPs).[9] For the same reasons, such a cellular cycling of K is essential for the propagation of action potentials in neuronal networks and muscle tissues. Beyond its direct implication in excitability of tissues, K is also crucial to a large range of vital functions, including the control of vascular tone and blood pressure, acid–base balance, the secretion and action of hormones, insulin and glucose metabolism, cell volume and intracellular osmolality, or secondary transport of solutes against their chemical gradients.[9–11,38]

The regulation of K in cells is key to many vital functions and the organism can rely on efficient systemic and cellular homeostatic mechanisms.[10,38,39,44] Endothermic vertebrates get their K exclusively from diet. Potassium is absorbed in the intestine and transferred from the digesta to blood plasma where it is continuously exchanged with all tissues. The vast majority of K intestinal absorption is balanced by the kidney via urinary losses.[40,44]

In the face of changing physiological or dietary conditions, the K homeostatic regulation system controls with high efficiency both the total body K content (external homeostasis) and the balance between intracellular and extracellular K stores (internal homeostasis).[10,11,39] The internal homeostasis maintains the plasma K levels (i.e. kalemia) within a narrow range of values (ca. 3.5–5 mmol/L in humans),[10,11] with large variations outside this range being deleterious to vital functions. Skeletal muscle and liver are primarily responsible for short term regulation of kalemia, with the balance of their K uptake and release being controlled by a hormonal system involving aldosterone, angiotensin, or insulin.[10,11] The external homeostatic system mainly modulates the balance between dietary inputs and urinary losses on longer terms.[10,11]

Possible controlling factors of K isotopes cycle in vertebrates

While the systematic distribution of K isotopes remains to be documented in endothermic vertebrates, it is possible to hypothesize the potential controls determining the variability of K isotope ratios in the various reservoirs involved in their K homeostasis.

First, as dietary K is the sole input to the organism, its isotopic composition is expected to be the primary driver of the K isotope compositions of the animal tissues. This relationship has been well documented and used in various metal stable isotope systems (e.g. Ca, Zn, Mg; see reviews).[3,6,7] However, the biological processing of K is expected to induce additional variability in the K stable isotope compositions of the animal tissues. The potential contribution of factors of physiological variability (e.g. species, age, sex) remains to be compared with the dietary controls.

Second, K cell homeostasis could affect the K isotope distributions at steady state or in response to varying environmental, physiological, or pathological conditions. The cellular cycling of K isotopes could introduce significant isotope fractionations, owing to the continuous and regulated transmembrane transport of K in animal cells. Sizeable mass-dependent fractionations of metal stable isotopes have previously been shown or suggested to result from transmembrane and transepithelial active or passive transports.[45–49] As a result, biological variations of internal K homeostasis in health or in disease, could be associated with distinct extra- vs. intracellular K isotope distributions. More generally, the external homeostatic regulation of the whole-body K stores could affect the K isotopes distributions, via the action of epithelia exchanging K with the environment.

Table 1. Summary of experimental design for controlled feeding experiments A and B[a]

	Species	Experimental diet	Number of (*n*) indiv.	Age at start	Body mass at start[b]	Experiment duration	Analysed material[c]
Exp. A	**Rat**	Plant-based pellets	3	11–12 wk	197 ± 22 g	5 d acclimatization +52–54 d on exp. diet	Diet, blood (plasma, RBC), skeletal muscle, heart (quails only), liver, bone, kidney, urine, feces
	Rattus norvegicus forma domestica	Meat-based pellets	3				
		Insect-based pellets	3				
	Guinea pig *Cavia porcellus*	Plant-based pellets	3	4–6 wk	398 ± 29 g		
		Meat-based pellets	3				
		Insect-based pellets	3				
	Quails *Coturnix japonica*	Plant-based pellets	3	7–8 wk	260 ± 49 g		
		Meat-based pellets	3				
		Insect-based pellets	3				
Exp. B	**First generation** (G1, sows)	Diet 1 (soya/fish: 100/0)	2	At weaning (≈7 wk)	≈10–15 kg	>18 mo	Diet, blood (whole, plasma), skeletal muscle, (femoral, loin), liver, milk (sows), feces, urine
Pigs (*Sus scrofa*)		Diet 5 (soya/fish: 0/100)	2				
	Second generation (G2, pigs)	Diet 1 (Soya/fish: 100/0)	3	*In utero* development	1.4 ± 0.4 kg at birth	160–190 d	
		Diet 2 (soya/fish: 87.5/12.5)	1				
		Diet 4 (soya/fish: 50/50)	2		15 ± 5 kg at weaning		
		Diet 5 (soya/fish: 0/100)	3				

[a]In experiment B, diets 1 to 5[52] refer to varying balances between soya bean and fish meal, contributing a constant 20 wt % protein content to the total diet. The soya/fish weight contributions (in %) are given together with each experimental diet number. Note: for experiment B, there are five diet formulations; however, tissues from the third diet formulation (75% soya/25% fish) were not used in this study.
[b]Uncertainties are 2SD over all individuals involved in this study.
[c]As available for this study, varies from a group to another.

This paper reports the first systematic exploration of the distributions of K isotopes in endothermic vertebrates to: (i) assess the role of diet in the determination of vertebrate isotope compositions, (ii) estimate the extent of interindividual variability across vertebrate species, (iii) identify the main cellular mechanisms responsible for K isotope distributions among different tissues, biofluids, and excreta, and (iv) propose a first model for the K isotope cycling in endothermic vertebrates.

To this end, K isotope compositions have been analysed in tissues, biofluids, and excreta of four different vertebrate species reared in two different controlled feeding experiments. The first experiment (experiment A) involved three different diets fed to adult female individuals of two mammalian rodent species (rats and guinea pigs) and one avian species (quails). The second experiment (experiment B) included individuals from two generations of pigs fed with either of five different diets. These experiments allow several potential factors of variability to be addressed, including possible different physiological effects across two classes of endothermic vertebrates (mammals and birds) and across different adult body masses. In contrast with experiment A, experiment B was performed over two successive generations, ensuring equilibrium of generation-2 tissues with their diets, even *in utero*, as disequilibrium is sometimes a limitation in feeding experiments.[50] Finally, pigs are recognized as very good analogues for humans although some differences persist, which serves the discussion for isotope metallomics.[50] The K isotope compositions of samples were measured together with international biological reference materials presented in this study for the sake of interlaboratory comparisons. Finally, a stable isotope box-modeling approach is developed to propose a first model of the K isotope homeostasis in vertebrates.

Material and methods

Supplementary material is available online and composed of Appendix A for supplementary text, Appendix B for figures and C for tables. Appendix D corresponds to the command files used in isotope box-modeling presented thereafter. Appendix E is the full dataset presented here.

Controlled feeding experiments

Experiment A: quails, guinea pigs, and rats

Experiment A involved adult female rats (*Rattus norvegicus* forma domestica, WISTAR RjHan: WI), guinea pigs (*Cavia porcellus*, Dunkin Hartley HsdDhl: DH), and quails (*Coturnix japonica*, from a private Swiss breeder) raised on three different diets for 52 to 54 d following a 5 d acclimatization period as previously described[51] (Table 1). The controlled feeding experiments were approved by the Cantonal Veterinary Office in Zurich, Switzerland (animal experiment license no. ZH135/16) and performed at the University of Zurich between July 2017 and January 2018.

The experiment was conducted using custom-made plant-, insect-, and meat-based isoproteic and isocaloric pellets. Each diet consisted of a primary ingredient, namely a lucerne meal (56 wt %), a lamb meal (25 wt %), and black soldier fly larvae insect protein meal (26 wt %) for the plant-, meat-, and insect-based diets, respectively.[51] The primary ingredient of each diet was blended with complimentary plant-derived ingredients, minerals, and vitamins to meet nutritional requirements.

The animals were housed in groups of three to six individuals and fed *ad libitum* with one of the three experimental diets and local tap water. On their arrival, the animals received their supplier diets, progressively replaced by experimental diet over a 5 d acclimatization period. Coprophagy was not prevented in rats or guinea pigs.[51] All animals were healthy over the duration of experiment A, and most feeding groups displayed a significant increase in body mass (Supplementary Fig. SB1 and Table SC1, respectively, in Appendices B of Supplementary figures and C of Supplementary tables). Some significant differences in growth performances across diets are observed, likely linked to differences in specific dietary requirements (Supplementary Table SC1).

At the end of experiment A, the animals were euthanized using carbon dioxide and immediately dissected for sampling of soft

and hard tissues, including liver, kidney, skeletal muscle (quadriceps), heart, blood plasma, RBC, and tibia bone. Urine and feces were collected in metabolic cages prior to death. All soft tissues were stored at −20°C. All soft tissues and feces were freeze-dried during 24 h before homogenization in a Retsch Cryomill, with the exception of biofluids (RBC, plasma, urine) that were kept frozen at −20°C.

Experiment B: pigs

Experiment B (Table 1) involved two successive generations of pigs (*Sus scrofa domesticus*) fed with one of five different experimental diets with various balances of soya bean vs. fish meal, contributing a constant 20% protein content in total diet (full description in Webb *et al.*).[52] This experiment was initially designed to study the effects of terrestrial vs. marine protein intake on carbon and nitrogen stable isotope compositions of pig tissues[50,52,53] as a proxy for archaeological marine resource exploitation. The soya bean and fish meal fractions of experimental diets also contribute other minerals, such as strontium[53] and potassium (this study). All diets are nutritionally equivalent and isoproteic.[50]

The experimental design has been previously described in detail elsewhere.[50,52,53] Briefly, the pigs were raised at Harper Adams University (Shropshire, UK) between 2010 and 2011. To ensure that a total equilibrium was reached between animal model and their diet, the controlled feeding experiment was carried out over two successive generations of pigs. A total of five pairs of sows (first generation, G1) was fed one of each experimental diet starting from their weaning (≈7 wk) until sacrifice as adults (>18 mo). The sows were artificially inseminated, and each gave birth to piglets (second generation, G2). The G2 pigs were fed on the same experimental diets as their mothers (including sow milk from the same dietary group) until sacrifice in adolescence (ca. 160–190 d). As previously discussed,[50] the weight gain of G1 and G2 pigs reflect no significant differences in growth performances nor health issues during the experiment. Overall, total weight gain showed no significant differences across dietary groups.

Following termination, samples were taken from key soft tissues, including liver and skeletal muscle (femoral and loin muscle), fluids (blood plasma, whole blood), and excreta (feces, urine). All samples were freeze-dried and soft tissues were homogenized by mincing. Milk samples were also taken and freeze-dried during the G1 sows lactating period.

Material

To characterize the K isotope homeostasis in these animal models, the key K bodily reservoirs as well as inputs and losses were sampled (Table 1). As diet is the only K input in endothermic vertebrates, all the powdered and homogenized pellets were sampled. Given the low K concentrations in drinking tap water (ca. 1 mg/L against ca. 3600 to 1600 µg/g in pelleted diet), it represents a negligible contribution to the total dietary K budget in endothermic vertebrates drinking freshwater, ranging from 0.05% to 0.4% of K daily intake.[39,54] The K isotope composition of drinking water was therefore not measured in this study. As skeletal muscle and liver are two major and key reservoirs in the K cycle, samples of both tissues were systematically taken from all individuals presented in this study. Other key reservoirs (plasma, RBC and whole blood, kidney, heart, bone, milk) and losses (urine and feces) were analysed from the different groups (species and dietary groups) depending on scientific relevance and on quantity remaining after initial studies on experiments A and B.

In experiment A, diet samples were taken from the three homogenized and powdered types of pellets (plant-, meat-, and insect-based pellets). In the three animal models (rats, guinea pigs and quails), a total of 99 samples were taken from the three different dietary groups with a focus on animals on the plant-based diet for the samples with limited availability.

In experiment B, the pigs included in this study belonged to four out of the five initial dietary groups (diets 1, 2, 4, 5, Table 1). In addition to samples from the four experimental diets, a total of 59 samples from 13 individuals were included. Of these, 45 samples were taken from nine G2 pigs (five males, four females) fed on either of the four selected diets. Whole blood samples are also included. In vertebrates, most of blood K (>94%) is found in RBC while plasma only contributes a small fraction, therefore, the K isotope compositions of whole blood can be considered equivalent to RBC.[40] To compare the K isotope homeostasis at two distinct ages and with different physiological states, 10 samples (femoral and loin skeletal muscle, liver) from four individuals of G1 pigs (sows) fed on either of the two end-member diets (diet 1 and diet 5) were included. Four milk samples from G1 pigs are also included. This allows an additional physiological K loss to be assessed as well as being the last dietary source of K before the final switch to direct consumption of the experimental diet in G2 pigs. In addition to femoral skeletal muscle samples, samples of loin skeletal muscle were also included for a subset of G1 and G2 individuals, to test for the influence of muscle type on K isotope compositions.

Finally, 10 reference materials have been included to assess the accuracy of the protocol for K isotope analysis and provide basis for future inter-laboratory comparisons. We included three geological reference materials: USGS BCR-2 basalt, SGR1B shale, IAPSO seawater. Also included are seven biological reference materials: BCR380R cow milk powder, BCR383 green beans, ERM CE464 tuna fish, NIST SRM 1400 cow bone ash, NIST SRM 1486 cow bone meal, NIST SRM 1577C bovine liver, and FBS fetal bovine serum (described in Albalat *et al.*[55] and Sauzéat *et al.*[56]).

Chemical processing

The K isotope compositions in samples and reference materials were measured using a protocol developed for biological and geological materials, briefly described here.

All sample preparation was carried out in the Bristol Isotope Group laboratory, University of Bristol, UK, under laminar flow hood and involved the use high purity reagents, namely 18.2 MΩ ultrapure water and trace-metal grade acids either purified by sub-boiling distillation (HNO_3, HCl), or commercially available (e.g. Romil Suprapur HF). All samples and reference materials selected were weighed and transferred to clean PFA beakers (15 ml Savillex). The typical digested masses ensured minimum content of 5–10 µg K. This typically corresponding to 5–10 mg of freeze-dried tissue or fluid samples (e.g. muscle, liver, blood plasma, whole blood, feces etc.), 30 mg of powdered pelleted diet, 30 mg of bone powder, around 80 µl fresh blood plasma, 20 µl fresh RBC, and 20 µl fresh urine. All biological samples and standards were digested using ca. 3 ml concentrated HNO_3 and 1 ml 30% Suprapur H_2O_2 in closed beakers at 130–140°C overnight. IAPSO Seawater aliquots (ca. 100 µl) were dried down in PFA beakers. The BCR-2 and SGR-1B silicate standards (ca. 30 mg) were digested in HF-HNO_3 at 200°C in high-pressure polytetrafluoroethylene bombs.[57] Following digestion, samples were evaporated to dryness on hotplate at ca. 100°C before being taken up in 1 N HNO_3 for ion exchange purification.

The chemical purification of K from the samples and reference materials was carried out in a two-step ion exchange chemistry developed for geological and biological materials. This protocol is summarized in Supplementary Table SC2 and typical elution curves of major and trace elements are shown in Supplementary Fig SB2. The first column (2.5 ml BioRad AG50W-X12 cationic resin, 200–400 mesh, internal diameter 7.5 mm) separates most of the matrix, and leaves only K with trace amounts of major elements such as Na and Mg. The second column (0.25 ml BioRad AG50W-X12 cationic resin 200–400 mesh, internal diameter 4 mm) further purifies K, removing residual matrix elements i.e. Na and Mg. As bone displays high Ca/K ratios (of the order of 1000), Ca^{2+} can possibly compete with K^+ and other cations on columns for sorption sites on the resin, potentially altering elution peak positions and compromising full recovery of K. Therefore, bone samples were purified twice on the first column. The first purification consisted in pooling the K bearing elution cut (step e, Supplementary Table SC2) together with the previous matrix bearing elution cut (step d), which could contain trace amount of K because of possible Ca competition. The second purification on the first column was performed normally. Potassium procedural blanks and recovery were assessed by measuring K elemental concentrations using the Thermo Fisher Scientific Element2 ICP-MS and the Proteus collision cell (CC)-MC-ICP-MS/MS.

The recovery of K from the chromatography procedure was estimated for geological and biological materials, and exceeds 99.5% of the loaded amount of K (as measured on mineral- and biological-like synthetic matrices, as well as aliquots of BCR-2 basalt and BCR383 green beans). Such a quantitative recovery is necessary so no chromatography induced mass-dependent isotope fractionation occurs.[58] The K blanks throughout the whole chemical processing (digestion and chromatography) did not exceed 20 ng. This is negligible when compared to the typical amount of K in processed samples and reference materials (typically ca. 5 to 100 µg K) and is not expected to affect accuracy of isotope ratio measurements beyond analytical precision. The efficiency of the purification was tested on the eight natural geological and biological reference materials by measuring the X/K molar ratios before and after the purification (where X is any major and trace element) using the Element2 ICP-MS mass spectrometer at the University of Bristol (UK). The results show X/K ratios are brought down to less than 0.01 for all major and trace elements (Supplementary Table SC3).

Several aliquots of most reference materials were chemically processed as replicates to check for accuracy and external reproducibility by replicating measurement of their K stable isotope compositions ($n = 2$–5 sample replicates). A 40 µg K aliquot of the SRM 3141a bracketing standard was also processed through both cation chemistries to further check for absence of any chromatography induced isotope fractionation.

Analytical methods

Elemental and isotopic analyses

Elemental concentrations of major essential elements, related to K homeostasis (K, Na, Mg, Ca, P) were measured in aliquots of all diet and animal samples by inductively coupled plasma optical emission spectrometry (ICP-OES) at the University of Bristol (UK) and at the Laboratoire de Géologie de Lyon, (France), following previously described methods.[59,60]

The K isotope compositions were measured at the University of Bristol using the Proteus prototype instrument developed by Thermo Fisher Scientific (Bremen) in collaboration with the Bristol Isotope Group. Proteus is a unique tribrid CC-MC-ICP-MS/MS with a pre-cell mass-filter. It has been previously described elsewhere.[61] The instrument combines a low energy front end, adapted from the Thermo Fisher Scientific iCAP Q instrument and consisting of a quadrupole mass pre-filter followed by a collision cell, and then a conventional Thermo Fisher Scientific Neptune plus analyser. The use of He collision and H_2 reaction gases in the collision cell allows a near-quantitative elimination of Ar^+ and ArH^+ beams,[62] which otherwise constitute major isobaric interferences hindering K isotopes analyses in low resolution and hot plasma conditions.[18,19,21,62]

Operating conditions for Proteus were optimized to minimize Ar^+ species formation while maximizing transmission and stability of K signal intensity and of $^{41}K/^{39}K$ ratios, as measured in standard solutions. A description of main settings is given in Supplementary Table SC4. Potassium isotope composition measurements were conducted on 1 mg L^{-1} purified K solutions diluted in 0.3 M HNO_3 and using a 50 µl/min PFA nebulizer in free aspiration mode connected to an Apex Q desolvating system (ESI). The mass pre-filter is operated in RF only mode allowing a wide range of masses to enter the collision cell (±40 amu).[63] Helium and hydrogen gases are introduced to the collision cell at 2 ml/min and 3.5 to 4 ml/min, respectively. The $^{39}K^+$ and $^{41}K^+$ beams on the Proteus multi-collector were measured on peak centre, in low resolution mode (measured resolving power $m/\Delta m \geq 3000$, 5–95% peak height definition[64]), on the L1 and H1 Faraday cups, respectively, using amplifiers fitted with $10^{11}\Omega$ resistors. Analysis of blank acid (pure 0.3 M HNO_3) shows very low K intensities, of the order of 70 to 100 mV of $^{39}K^+$ while K solutions yielded signal intensities of ca. 30 V/mg L^{-1}. Helium and hydrogen collision and reaction gases efficiently reduce the $^{40}Ar^+$ beam intensity on central cup from about 3000 to 4000 V to less than 2 mV in blank 0.3 M HNO_3 acid. This corresponds to a near-quantitative suppression of the Ar^+ beam by more than six orders of magnitude. Formation of $^{40}ArH^+$ hydrides interfering with $^{41}K^+$ is also negligible, with measured intensities comparable to expected blank levels based on the $^{39}K^+$ signal, ≈6 mV, while K solutions yielded $^{41}K^+$ signal intensities of ca. 2 V/mg L^{-1} (0.130 V/mg L^{-1} for $^{39}K^+$).

Isotope ratios were measured using the standard-sample bracketing (SSB) method for correction of instrumental mass bias[65] with NIST SRM 3141a used as a bracketing standard. The K stable isotope compositions are expressed in ‰ using the delta notation, defined as follows:

$$\delta^{41}K_{SRM3141a} = \left(\frac{^{41}K/^{39}K_{sample}}{^{41}K/^{39}K_{SRM3141a}} - 1\right) \times 1000, \quad (1)$$

where $^{41}K/^{39}K$ refers to the measured abundance ratios. Each sample and standard measurement was preceded by a washout (200 s) and a blank measurement of 0.3 M HNO_3. Sample and standard measurements consisted of 40 cycles with 8.389 s integration times (10 cycles in blank). Blank contributions were corrected online. Sample measurements were bracketed by measurement of NIST SRM 3141a. Each measurement required ca. 300 ng K, corresponding to the uptake of ca. 300 µl of a 1 mg/L^{-1} K solution. Measurements (full SSB cycle) were replicated at least three times on the same purified solution for all samples and reference materials.

Precision and accuracy of K isotope ratio analyses

The pure SRM 3141a solution was regularly analysed as a sample bracketed against itself over a period of 20 mo and has a mean

Table 2. δ^{41}K values of all analysed reference materials[a]

		$\delta^{41}K_{SRM3141a}$ (‰)				
	Material	**Mean**	**2SD**	**95% C.I.**	***n***	***N***
SRM3141a purified	This study (D1X1)	−0.01	0.11	0.02	25	-
BCR2	This study (D2X2)	−0.45	0.09	0.02	25	-
Basalt	This study (D2X3)	−0.43	0.12	0.06	6	-
	This study (D2X4)	−0.45	0.14	0.04	15	-
	Mean of replicates	**−0.44**	0.03	0.00	-	3
	Lit. mean (BCR 1 and 2) (1–9)	**−0.43**	0.05	0.02	-	11
BCR380R	This study (D3X10)	0.07	0.03	0.02	5	-
Cow milk powder	This study (D3X18)	0.06	0.04	0.03	4	-
	This study (D3X3)	0.07	0.11	0.04	11	-
	This study (D3X9)	0.07	0.03	0.03	3	-
	Mean of replicates	**0.07**	0.01	0.01	-	4
	Lit. mean (9)	**0.07**	0.02	0.09	-	2
BCR383	This study (D3X3)	−0.80	0.07	0.03	7	-
Green beans	This study (D3X4)	−0.86	0.10	0.05	7	-
	This study (D3X8)	−0.80	0.07	0.02	16	-
	Mean of replicates	**−0.82**	0.06	0.08	-	3
	Lit. mean (9)	**−0.84**	0.07	0.31	2	-
CE464	This study (D3X14)	0.29	0.06	0.05	4	-
Tuna fish	This study (D3X3)	0.29	0.08	0.03	9	-
	This study (D3X9)	0.29	0.06	0.02	9	-
	Mean of replicates	**0.29**	0.00	0.01	-	3
	Lit. mean (9,10)	**0.34**	0.08	0.10	-	3
FBS	**This study** (D3X3)	**−2.04**	0.05	0.03	5	-
Fetal bovine serum	**Lit. mean** (9)	**−2.11**	-	-	1	-
Seawater	This study (D1X1)	0.12	0.09	0.02	32	-
(IAPSO)	This study (D11X12)	0.12	0.08	0.04	7	-
	This study (D4X4)	0.11	0.10	0.02	22	-
	This study (D8X8)	0.14	0.05	0.01	23	-
	This study (D11X20)	0.16	0.04	0.02	6	-
	Mean of replicates	**0.13**	0.03	0.02	-	5
	Lit. mean (seawater) (2, 4, 6–9)	**0.11**	0.07	0.02	-	10
SGR1B	This study (D3X12)	−0.27	0.03	0.04	3	-
Shale	This study (D3X3)	−0.23	0.08	0.03	9	-
	Mean of replicates	**−0.25**	0.05	0.22	-	2
	Lit. mean (SGR1) (1, 2, 4–5, 8, 9)	**−0.27**	0.04	0.02	-	7
SRM1400	This study (D10X11)	−0.22	0.07	0.05	5	-
Cow bone ash	This study (D11X13)	−0.19	0.11	0.07	5	-
	This study (D11X21)	−0.16	0.05	0.02	8	-
	Mean of replicates	**−0.19**	0.06	0.07	-	3
SRM1486	This study (D11X13)	−0.57	0.12	0.04	10	-
Cow bone meal	This study (D10X21)	−0.53	0.06	0.03	8	-
	Mean of replicates	**−0.55**	0.05	0.24	-	2
SRM1577C	This study (D3X3)	0.13	0.12	0.04	10	-
Bovine liver	This study (D3X7)	0.16	0.08	0.04	8	-
	Mean of replicates	**0.15**	0.04	0.18	-	2
	Lit. mean (9)	**0.15**	0.00	-	2	-

[a]Each sample line refers to the mean of the repeated measurements of a given sample that underwent chemical processing. The sample is referred to using its D digestion number (e.g. D1) and X chemistry number (e.g. X1). *n*: number of replicated analyses on a single sample; *N*: number of samples analysed (1:[69]; 2:[18]; 3:[17]; 4:[15]; 5:[24]; 6:[19]; 7:[36]; 8:[70]; 9:[71], 10:[30]).

δ^{41}K value of 0.000 ± 0.066‰ (2 SD, $n = 416$, 2 SE = 0.003‰), indistinguishable from the theoretical 0‰ value. The external reproducibility was assessed by using the pooled standard deviation of repeated analyses of the reference materials processed through column chemistry over a period of 20 mo (Table 2). This assessment allows multiple chemical processing of reference materials (digestions, chemical purification) measured over numerous analytical sessions to be combined to give a robust estimation of the reproducibility. More details can be found elsewhere.[66–68] The pooled double standard deviation (2 SD) over all chemically processed reference materials analysed in this study was 0.048‰. Such a reproducibility is comparable to the most precise

methods published so far with collision cell MC-ICP-MS[18,19] or with enhanced resolution.[17]

The measured reference materials are shown in Table 2 together with compositions compiled from literature. The δ^{41}K of the purified aliquot of SRM 3141a standard is undistinguishable from the expected 0‰ value (−0.01 ± 0.02‰, 95% C.I., $n = 25$) and shows that no measurable isotope fractionation is induced by chemical processing. The geological reference materials with previously published isotope compositions show very good agreement with literature mean values, as is the case for BCR2 basalt, SGR1-B shale and IAPSO seawater. Our analyses also further characterize five biological reference materials recently described in two publications,[30,71] namely BCR380R milk powder, BCR383 green beans, CE464 tuna fish, FBS fetal bovine serum and SRM1577C bovine liver. Finally, we present here the first isotope compositions to date measured in two cow bone reference materials, namely SRM1400 (−0.19 ± 0.06‰, 2SD, $n = 3$ sample replicates) and SRM1486 (−0.55 ± 0.05‰, $n = 2$).

Statistical analyses

Statistical analyses were performed using R.[72] Depending on the type of analysis and dataset, different statistical tests were applied. Linear correlations were explored using parametric Pearson correlation test (noted Pear.) or nonparametric Spearman rank sum test (Spear.). Differences in the mean values of multiple groups were tested using parametric Welch's ANOVA test (WA) or nonparametric Kruskal–Wallis test (KW). Differences between two groups were tested using parametric Welch's *t*-test (W) or nonparametric Wilcoxon–Mann–Whitney test (WMW). Finally, mean compositions of single groups were compared to a theoretical 0 mean value using the one-sample *t*-test (o.s. *t*-test). The *P*-values (*P*) are given together with the degree of significance denoted by asterisks as follows: NS (nonsignificant, $P > 0.1$), ($P < 0.1$), * ($P < 0.05$), ** ($P < 0.01$), and *** ($P < 0.001$). Unless otherwise stated, all uncertainties associated with a mean isotope composition refer to the 95% confidence interval (C.I.) calculated using the *t*-test. Statistical reports are provided as tables in appendix C of supplementary information (Supplementary Tables SC5 to SC12) and are systematically referenced in the captions of figures they refer to, and vice versa.

Stable isotope box models of K cycle in vertebrates

Isotopic equilibration model

The duration of the controlled feeding experiments A and B are different, and both involve changes of K dietary sources. A transition from one diet to another could induce a change in the δ^{41}K values of the dietary source. Moreover, the residence times of K vary across the different bodily reservoirs.[40] As the aim of this study is to characterize the steady-state distributions of K isotopes, the progress of the isotopic equilibration of the animal tissues with their dietary K needs to be assessed. While a large corpus of studies report the kinetics of K transport in specific tissues,[40] no study has reported the typical systemic equilibration patterns of bodily K with dietary K. To characterize the isotopic equilibration of the organism to its diet, we build a box-model representative of an endothermic vertebrate organism, following a similar approach as previously described for Ca or Zn isotopes.[73,74] This isotopic equilibration model aims at estimating the order of magnitude of the characteristic relaxation times for the system to isotopically equilibrate with the dietary source (Appendix A, Text A.1).

A full description of the method and program used for this purpose is given in supplementary information (Appendix A, Text A.1, Section A.1.1.1., Supplementary Fig. SB3.A, Table SC13). Data from a thorough model of the K cycle in humans previously published by Leggett and Williams (1986)[40] is used as starting point. Using this description of the K cycle in an adult human organism, a box model of the cycle of K isotopes in this system has been adapted using the isobxr R package.[75] Simulations of the response of the system to a change in dietary isotopic composition have been run without isotopic fractionation. As detailed in appendix A.1 of supplementary information, the use of such a K cycle pattern allows the estimation of the order of magnitude of K equilibration timing for endothermic vertebrates with similar K cycle patterns, assuming a first order isometry of the K fluxes together with the sizes of the K reservoirs across animals with varying body masses. Our isotopic diet–body equilibration box model was benchmarked by comparing simulations of K isotope tracer studies with simulations of Leggett and Williams (1986) and with independent data from tracer studies in human (Supplementary Fig. SB4.A). The very good agreement between our simulations and experimental data as well as previous models shows that our isotopic equilibration model accurately reproduces the K cycle and its dynamic. This model can hence be used to discuss the dynamic isotopic equilibration of animal tissues with diet and between reservoirs themselves.

K isotope homeostasis model

A stable isotope box model to assess the physiological controls over steady-state isotope homeostasis has been developed (detailed description in Appendix A, Text A.1., Section A.1.2.1.). This K isotope homeostasis box-modeling approach consists in calculating the evolution of distributions of K and its isotopes in all interconnected boxes of the system, forcing the simulations with box sizes (masses of K), fluxes (mass of exchanged K per time unit) and associated isotope fractionations (defined as isotope fractionation factors).

Here, we use the extensively described cycle of K in adult humans.[9,38,44] in a simplified version of the model presented earlier[40] (Supplementary Fig. SB3.B, Table SC14.A). The flux configurations used for steady-state simulations allow a wide range of variability of the K fluxes in the organism to be covered (Supplementary Table SC14.B). To this end, two series of six flux configurations were set to test the effects of variable intestinal absorption and variable renal excretion onto steady-state K isotope distributions in a balanced organism (i.e. no net loss or gain of K in any reservoir). The simulations of K isotope distributions were calculated using the isobxr R package.[75] All input parameters, codes and outputs are made available in supplementary information.

Results

Diet–body equilibration model

The results of the isotopic diet–body equilibration simulations are presented in detail in Appendix A, Text A.1., Section A.1.1.2. The first equilibration simulation characterizes the isotopic cross-equilibration between all key bodily reservoirs (Supplementary Fig. SB4.B). These results show that skeletal muscle drives the dynamics of the whole internal system. All other internal reservoirs [i.e. except gastro-intestinal tract (GIT) and feces] tend to equilibrate with muscle within ca. 10 d, which itself displays the slowest response equilibration pattern. This is expected as muscle K content is one order of magnitude higher than any other bodily reservoir (70–75% of body K) and

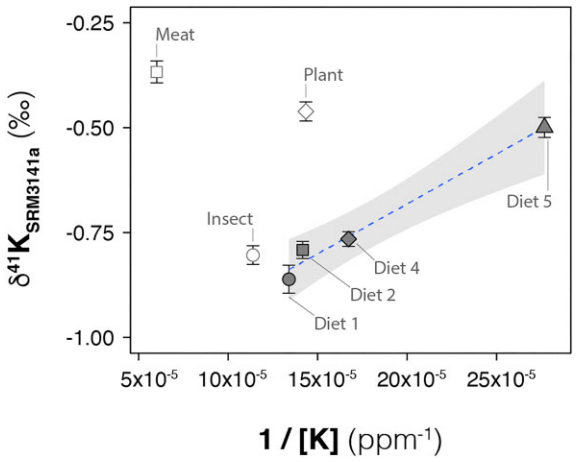

Fig. 1 $\delta^{41}K$ values of dietary K (‰, relative to SRM3141a) as a function of the inverse of K concentrations (ppm^{-1}). Empty and full symbols refer to experiment A and B, respectively. Error bars are 95% confidence intervals (C.I.). Diets 1, 2, 4, and 5 of experiment B fall on a mixing line (dashed blue line with 95% C.I. shaded area) with a significant correlation (Pear. $R^2 = 0.982$, P-value = 0.009 **). Corresponding data is shown in Supplementary Table SC5.

the residence time of K in muscle alone is the second longest (≈9 h), behind red blood cells (≈64 h). The other reservoirs are thus expected to be at equilibrium with muscle before reaching equilibrium with diet. Skeletal muscle is hence a useful internal reference for the study of distribution of K isotopes in endothermic vertebrate organisms.

The second equilibration simulation was performed to estimate the timing of whole-body equilibration to a change in diet isotope composition (Supplementary Fig. SB4.C). Such an equilibration can be described by characteristic relaxation times of the summed exponential differential equations solutions. The longest relaxation time of the system provides a characteristic time for the long-term diet–body equilibration, and hence offers a measure of the whole-body residence time of K. Our results show that the whole-body relaxation time of K is of the order of 40 to 50 d. At about 50 d, all bodily reservoirs reach ca. 60% of the full equilibrium, 90% at 100 d and 96% at 150 d.

K isotope compositions of experimental diets

The K isotope compositions of diets are shown in Fig. 1. Experiment A diets display significantly different compositions and span a total range of 0.43‰. Experiment B diets also display significant differences over the range of soya and fish meal mixes, spanning a similar range (0.36‰). The $\delta^{41}K$ mean values of experiment B diets fall on a mixing line when plotted against the inverse of K concentrations (Pear. $R^2 = 0.982$, $P^{**} = 0.009$). Experiment B diet K concentrations also fall on a mixing line when plotted against the fraction of fish protein (Pear. $R^2 = 0.985$, $P^{**} = 0.007$, Supplementary Table SC5). The fish meal and soya in the experiment B diets hence contribute two isotopically distinct K dietary sources: a ^{41}K-enriched marine endmember and a ^{41}K-depleted soya endmember. This is in good agreement with the documented dichotomy between ^{41}K-enriched marine animal vs.^{41}K-depleted terrestrial plants.[29]

Distributions of K stable isotopes in animal tissues

All K isotope compositions of animal samples are shown in Supplementary Fig. SB5. Overall, the 158 samples display $\delta^{41}K$ values spanning a range of 1.62‰, between −0.88‰ and 0.74‰.

Correlations between bodily reservoirs and with dietary $\delta^{41}K$

The isotopic equilibrium between animal tissues was first assessed. The Supplementary Fig. SB6 shows the $\delta^{41}K$ of all reservoirs against those of skeletal muscle taken as an intraindividual reference. A systematic and significant correlation for liver is observed in each species. In addition, the slopes of these linear regressions are compatible with 1. The same holds for kidney of quail, rat, and guinea pig. Depending on counting statistics, linear correlations appear more variable, being either significant when pooling species (blood plasma, RBC) or poorly to nonsignificant (heart, bone, urine, feces, milk) owing to a lack of statistical power. Overall, the slopes of these regressions tend to be positive and to parallel the identity line.

The equilibration of the animal tissues with diet is tested by comparing dietary $\delta^{41}K$ of diet with $\delta^{41}K$ of skeletal muscle and liver (Fig. 2). The pigs, from experiment B, display the strongest and most significant correlation with diet in both muscle and liver and the slopes of these linear regression lines are compatible with 1. By contrast, the results from experiment A are more variable. Guinea pigs display strong and significant correlations for both muscle and liver (Pear. $R^2 = 0.56$, $P^* = 0.021$ and $R^2 = 0.55$, $P^* = 0.023$, respectively) and the slopes are also compatible with 1 (1.23 ± 0.83 and 1.07 ± 0.73, 95% C.I., respectively). The distributions seem more variable, however, as exemplified by the low $\delta^{41}K$ values in the tissues of the guinea pigs fed on the meat-based pellets (diamonds in Fig. 2). Quails display no significant positive correlation of their muscle or liver compositions with diet (the latter potentially owing to a smaller number of samples), although the trends are compatible with a slope of 1. Finally, the rats display no significant trends and seem incompatible with a 1:1 relationship.

Normalizations and reservoir-specific distributions

The $\delta^{41}K$ values of tissues are normalized to an individual's diet or skeletal muscle isotope compositions to correct for dietary controls or interindividual variability, respectively. This is referred to as normalization to diet or skeletal muscle and expressed in Δ notation[76] as:

$$\Delta^{41}K_{Diet} = \delta^{41}K^{sample}_{SRM3141a} - \delta^{41}K^{diet\ x}_{SRM3141a} \quad (2)$$

$$\Delta^{41}K_{Muscle} = \delta^{41}K^{sample}_{SRM3141a} - \delta^{41}K^{indiv\ skel.\ muscle}_{SRM3141a} \quad (3)$$

The tissue specific distributions of $\Delta^{41}K_{Diet}$ and $\Delta^{41}K_{Muscle}$ values are presented for each species in Fig. 3 and for all species pooled together in Fig. 4. The exhaustive distributions grouped by species, diet and tissue are shown in Supplementary Fig. SB5.

For a given reservoir, the diet-normalized compositions ($\Delta^{41}K_{Diet}$) display overall a reduced variability when compared to the $\delta^{41}K_{SRM3141a}$ distributions in guinea pig, quails, and pigs, while the rats seem to follow an opposite trend (Supplementary Fig. SB5). Normalization to muscle ($\Delta^{41}K_{Muscle}$) further reduces interindividual variability in a vast majority of K reservoirs in comparison with diet-normalized distributions. This is statistically supported by Bartlett tests for equality of variances, which yield statistically significant results in key reservoirs with high counting statistics, at the species level and across all species (Supplementary Tables SC8, SC9).

When comparing species (Fig. 3), the normalized compositions of K reservoirs yield comparable distributions, although some significant differences can be observed. The $\Delta^{41}K_{Diet}$ and $\Delta^{41}K_{Muscle}$

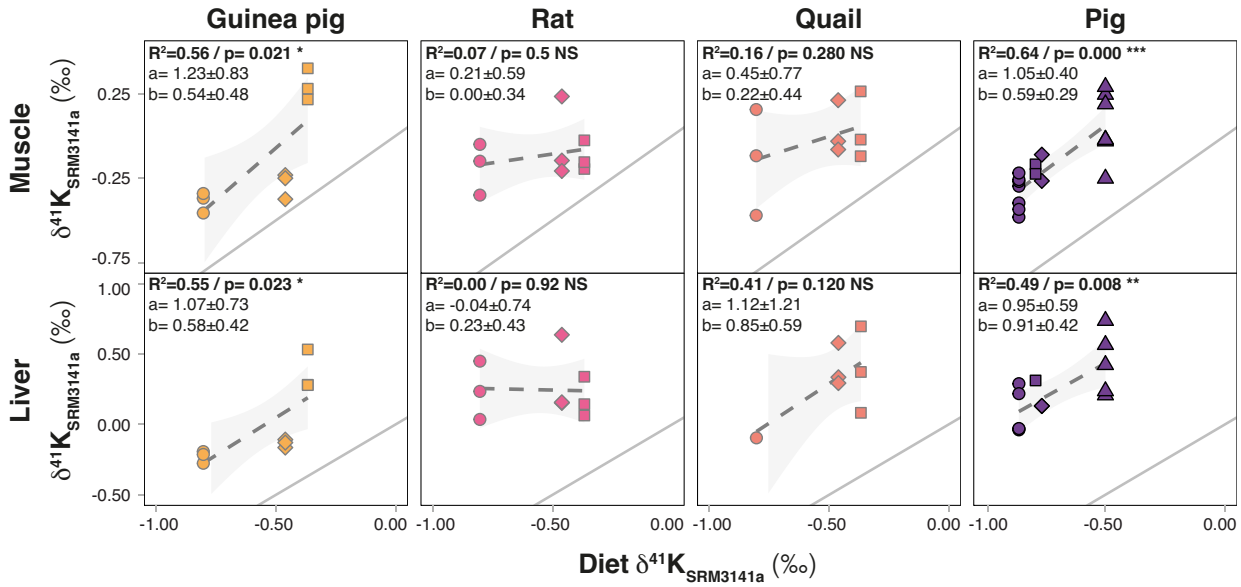

Fig. 2 $\delta^{41}K$ of skeletal muscle and liver vs. diet $\delta^{41}K$. Expressed in ‰ relative to SRM3141a. Gray continuous line is the identity 1:1 line. The dashed gray line is the regression line shown with 95% C.I. shaded area. Linear model statistics are given with the squared correlation coefficient (R^2), the regression *P*-value, and values of the slope (a) and y-intercept (b) together with their 95% C.I. For experiment A animals (guinea pig, rat, quail), circles refer to individuals fed on insect-based diet, diamonds to meat-based diet and squares to plant-based diet. For experiment B (pigs), circles correspond to diet 1 (soya/fish: 100/0), squares to diet 2 (87.5/12.5), diamonds to diet 4 (50/50), triangles to diet 5 (0/100). Full statistical report is shown in Supplementary Table SC7.A.

distributions across species are described in detail in supplementary information (Appendix A, Text A.2.). Overall, the normalized compositions of animal tissues are primarily dependent on the type of reservoir considered and not on the species. In pigs, while sex is not a clear factor of variability, we observe a possible difference in isotope compositions of the liver between generations G1 and G2 (Supplementary Fig. SB8). Pooling all species together (Fig. 4), the isotope compositions of K reservoirs display significant differences of their mean compositions, both for $\Delta^{41}K_{Diet}$ (WA: $P^{***} < 10^{-4}$, $F = 22.9$, df = 9; KW: $P^{***} < 10^{-4}$, df = 9, $n = 158$) and $\Delta^{41}K_{Muscle}$ (WA: $P^{***} < 10^{-4}$, $F = 41.4$, df = 9, KW: $P^{***} < 10^{-4}$, df = 9, $n = 158$). Urine and blood plasma appear to be the most depleted reservoirs, while all organs as well as feces and milk display ^{41}K-enriched isotope compositions.

Discussion

Diet–body isotope equilibrium and dietary control

A first goal of this study is to assess the contribution of diet to the isotopic variability across individuals' tissues for a given species. Such an approach relies on the assumption that animal tissues are isotopically equilibrated with experimental diets. Both experiments involve dietary transitions. The animal tissues could thus reflect varying stages of diet–body isotopic equilibration. We therefore first assess the progress of isotopic equilibrium between diet and animal tissues.

The progress of isotopic equilibration can vary from a reservoir to another because the residence times of K are variable across reservoirs. According to the outputs of the equilibration box model (Appendix A, Text A.1., Section A.1.1.2.), the K reservoirs are expected to isotopically equilibrate with one another and with skeletal muscle within a short period of ca. 10 d (Supplementary Fig. SB4.B). Our simulations also show that muscle primarily drives the long-term dynamics of the whole system. As a result, most tissues are expected to be equilibrated with one another and with muscle by the end of both experiments, since those exceed such a characteristic time. This is supported by the rather coherent and globally significant 1:1 linear relationships observed between most key reservoirs, such as liver and kidney, with muscle $\delta^{41}K$ values (Supplementary Fig. SB6), despite some contrasting counting statistics. We therefore consider that there is a globally good isotopic equilibrium of animal tissues with skeletal muscle.

Both sets of experimental diets have $\delta^{41}K$ values ranging over a 0.40‰ range, allowing us to test the control of diet on bodily reservoirs. When plotting $\delta^{41}K$ values of skeletal muscle or liver against those of experimental diets for each species, experiment A animals display variable degrees of linear correlation with diet (Fig. 2). While equilibrium distributions are expected to tend to a 1:1 relationship between a given reservoir and diet, the observed correlations suggest that pigs, guinea pigs and quails are better equilibrated than rats. Overall, experiment A species seem to be only partially equilibrated with their diets. Contrastingly, experiment B pigs display a strong and statistically significant 1:1 linear relation with their experimental diets. Pigs are thus fully equilibrated with their experimental diets and the isotope composition of diet controls those of their tissues.

The differences in diet–body isotopic equilibration are probably linked to the distinct experimental durations. This is notably supported by the diet–body isotopic equilibration model. The adult endothermic vertebrate organism is characterized by a typical whole-body relaxation time of ca. 50 d (Supplementary Fig. SB4.C). During this period, comparable to experiment A duration, the organism is only partially equilibrated with diet, reaching ca. 60% of its full diet–body isotopic equilibrium. Contrastingly, experiment B lasted more than 160 d in G2 pigs and 18 mo in G1, which would lead to full equilibrium for both generations.

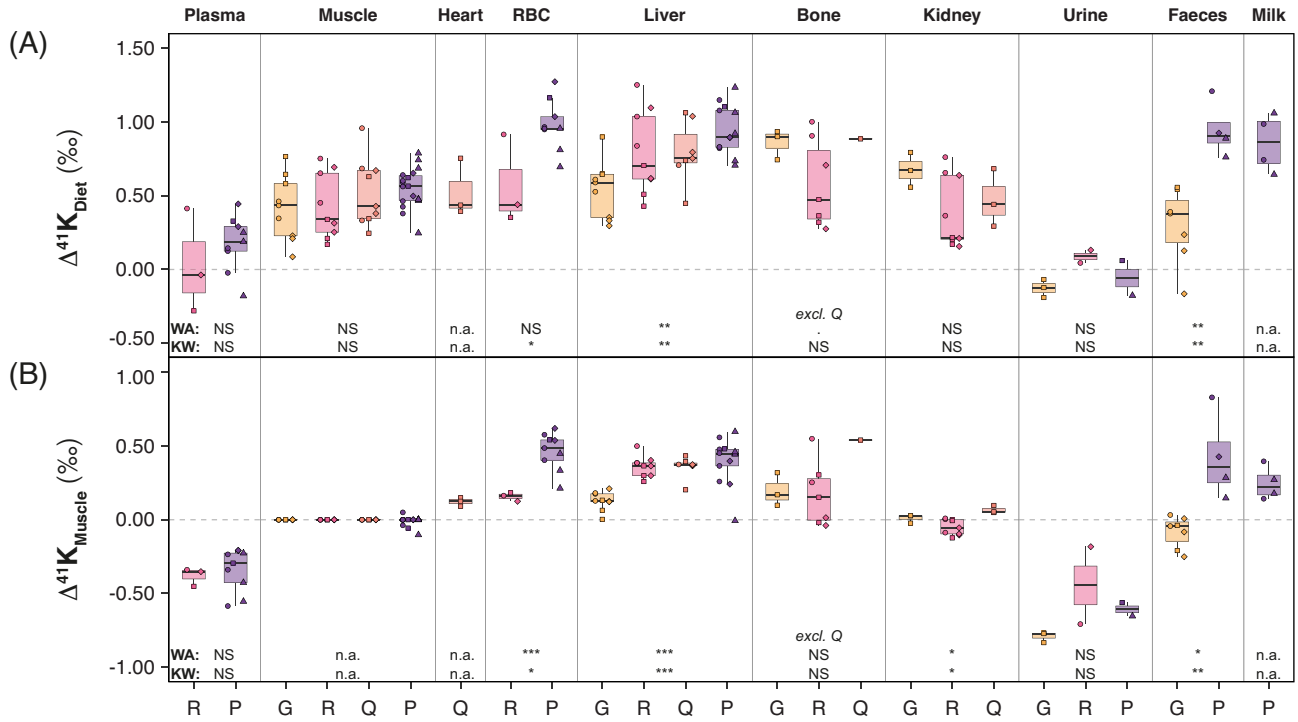

Fig. 3 Interspecific distributions of normalized K isotope compositions in all compartments (G: guinea pig, R: rat, P: pig, Q: quail), expressed relative to diet (A, $\Delta^{41}K_{Diet}$) and to each individual own skeletal muscle (B, $\Delta^{41}K_{Muscle}$). The boxplots indicate the 5%, 25%, 50%, 75%, and 95% quantiles. The significance levels of the *P*-values calculated from the Welch's ANOVA test (WA) and from the Kruskal–Wallis test (KW) are shown when number of groups allows (n.a.: not available, NS: nonsignificant *P*-value;. : $P = 0.05–0.1$; * : $P = 0.01–0.05$; ** : $P = 0.001–0.01$; *** : $P < 0.001$). Descriptive and comparative statistics are shown in Supplementary Table SC8. In pigs, $\Delta^{41}K_{Muscle}$ were calculated using the femoral skeletal muscle of all individuals, loin muscle was measured in four individuals. The latter appear as nonzero values in the $\Delta^{41}K_{Muscle}$ of pig muscle. For experiment A animals (guinea pig, rat, quail), circles refer to individuals fed on insect-based diet, diamonds to meat-based diet and squares to plant-based diet. For experiment B (pigs), circle correspond to diet 1 (soya/fish: 100/0), squares to diet 2 (87.5/12.5), diamonds to diet 4 (50/50), triangles to diet 5 (0/100).

These observations are further supported when evaluating the influence of the gain in body mass during experiments. The body mass gain (BMG) over the period of experimental feeding can be considered a measure of the extent of replacement of the initial K store (at equilibrium with the previous dietary source) by K taken from experimental diet. The K stores are expected to increase with body mass, inducing a faster replacement of pre-experimental K stores. Therefore, an incomplete replacement of initial K stores below a certain BMG threshold value would result in variable $\Delta^{41}K_{Diet}$ values for a given reservoir and would depend on BMG. In case of a full diet–body equilibrium beyond a given experiment duration or a BMG threshold, we expect $\Delta^{41}K_{Diet}$ to be insensitive to total BMG. On average, all animals gained weight since their last dietary transition from supplier diet (experiment A, BMG increase by up to 200%, Supplementary Fig. SB1) or mother's milk (experiment B, BMG increase by up to 1100%.[50]). In pigs, the $\Delta^{41}K_{Diet}$ values of skeletal muscle or liver display no significant dependence on BMG and the slope estimates are compatible with 0 (Supplementary Fig. SB7). By contrast, muscle and liver $\Delta^{41}K_{Diet}$ of guinea pigs and rats are significantly and positively correlated with BMG. Similar yet nonsignificant trends are observed in quails likely owing to a poorer representation of low BMG individuals. Experiment A individuals with the highest BMG display $\Delta^{41}K_{Diet}$ comparable to those of pigs, known to be at equilibrium, while those with low BMG display lower $\Delta^{41}K_{Diet}$ values. Experiment A individuals with the best growth performances are thus closer to a full isotopic equilibrium with their dietary source. The isotopic equilibration of experiment A animals is thus variable and depends on growth performances while pigs are considered fully equilibrated with their diet.

To summarize, the evaluation of dietary controls allows to draw three conclusions. First, the isotope composition of diet constitutes the primary control over isotope compositions of the animal tissues. This constitutes a solid basis for the use of K isotopes to reconstruct dietary habits in vertebrates. Moreover, experiment B suggests that K isotopes bear the potential to differentiate between marine and terrestrial dietary sources, as their isotopic dichotomies are directly reflected in pig tissues. Second, the normalization to experimental diet ($\Delta^{41}K_{Diet}$) allows to efficiently reduce the spread of isotope compositions contributed by dietary sources of K, except for groups with individuals displaying an incomplete diet–body isotopic equilibrium owing to low BMG. This normalization is therefore used thereafter to discuss the diet–body isotope fractionation effects, although considered more adequate for groups with overall full diet–body equilibrium such as pigs. Finally, the normalization to skeletal muscle ($\Delta^{41}K_{Muscle}$) allows to internally correct for interindividual variability possibly driven by incomplete diet–body isotopic equilibrium. This normalization produces consistent intra-organism distributions of K isotopes as exemplified by the reduced spread of $\Delta^{41}K_{Muscle}$ values in most reservoirs when compared to $\Delta^{41}K_{Diet}$ (Supplementary Tables SC8, SC9). Normalization to muscle is therefore used thereafter to discuss intra-organism distributions of K isotopes.

Biological factors of variability

Potassium isotope compositions vary widely within and across individuals. This is illustrated by the distributions of $\Delta^{41}K_{Muscle}$ values, varying from -0.64 ± 0.20‰ in urine to 0.39 ± 0.11‰ in RBC (Fig. 4). Overall, such a 1‰ intraindividual range is remarkable as

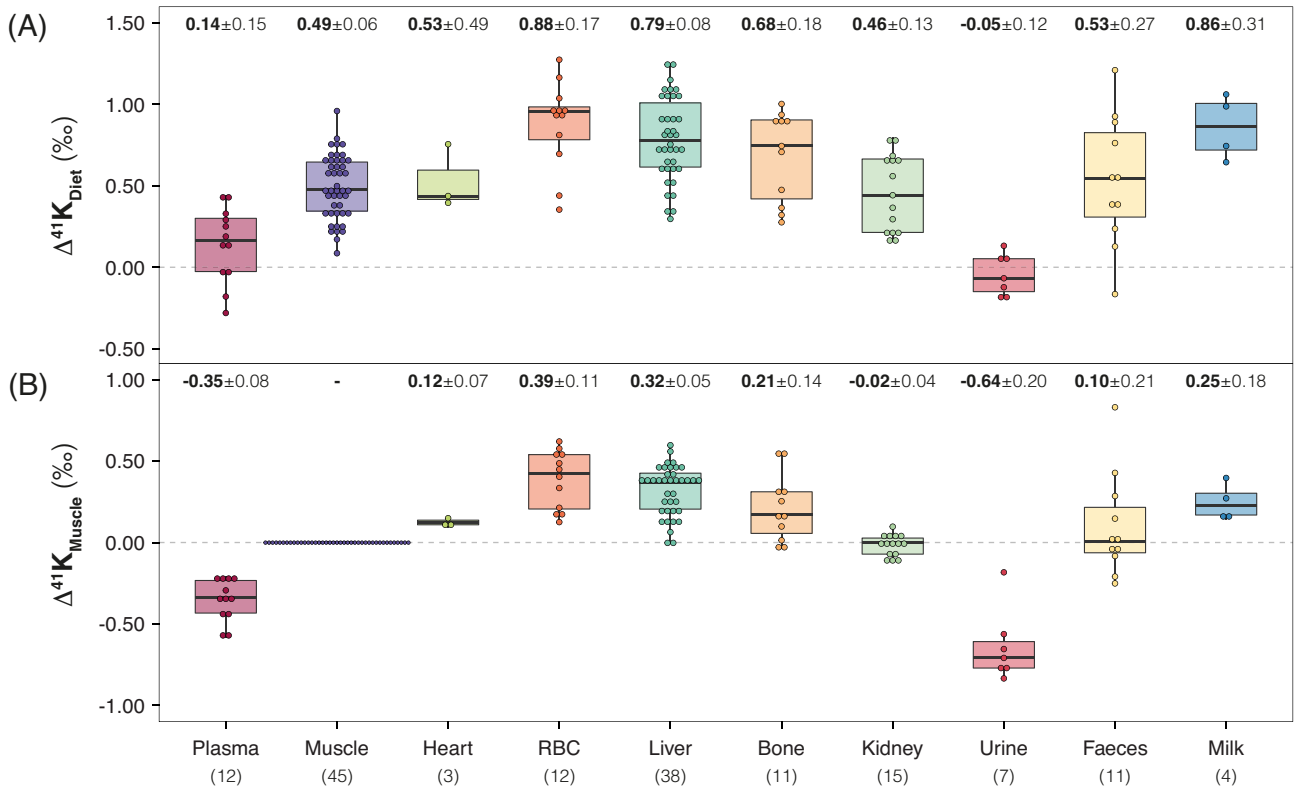

Fig. 4 Distributions of K isotope compositions of all measured tissues, biofluids and excreta in all taxa expressed relative to diet (A, $\Delta^{41}K_{Diet}$) and to each individual's own skeletal muscle (B, $\Delta^{41}K_{Muscle}$). The boxplots indicate the 5%, 25%, 50%, 75%, and 95% quantiles. The Welch's ANOVA and Kruskal–Wallis tests show significant differences of the means of all reservoirs, for $\Delta^{41}K_{Diet}$ (Welch's ANOVA *P*-value $<10^{-4}$, $F = 22.9$, df = 9; Kruskal–Wallis *P*-value $<10^{-4}$, df = 9, $n = 158$) and $\Delta^{41}K_{Muscle}$ (Welch's ANOVA *P*-value $<10^{-4}$, $F = 41.4$, df = 9, Kruskal–Wallis *P*-value $<10^{-4}$, df = 9, $n = 158$). Descriptive and comparative statistics are shown in Supplementary Table SC9. The mean compositions (in bold) and the associated 95% confidence interval values are given for each distribution. The numbers of samples for each reservoir are shown below.

it compares with the variability observed across Earths major geological K reservoirs.[29] This spread is directly comparable to the variability reported for other period four metals in vertebrates (Cu, Fe, Zn, Ca[2-5,77,78]). The biological processing of K by vertebrates is therefore responsible for major and maintained fractionations of K isotopes. Such sizeable so-called "vital effects" highlight the potential of K isotopes in the study of K homeostasis, and for applications both in isotope metallomics and paleobiology.

Intraindividual variations in $\delta^{41}K$ primarily depend on the type of bodily reservoirs and excreta (Fig. 4). However, further biological factors could also contribute to the variability documented for each K reservoir (Fig. 3). We studied three mammalian and one avian taxa with distinct physiological traits possibly influencing their K isotope cycling. Age or sex could also contribute to this variability. While the systematics of K isotope distributions appears to be globally shared by the species included in this study, some level of variability could be related to such factors (Appendix A, Text A.3. of supplementary information). We notably report distinct distribution of guinea pig liver isotope compositions that could relate to digestive physiology. Also, RBC are possibly sensitive to differences in physiological traits, such as RBC lifespans, membrane permeability and metabolism. However, no major effect of age, sex or possible basal differences of K metabolism is reported based on the current data.

Overall, the similar distributions of K isotopes across reservoirs show that K isotope cycling primarily depends on globally shared isotope fractionation mechanisms among endothermic terrestrial vertebrates. Indeed, the normalized compositions of a given reservoir yield similar distributions in the four taxa, including in tissues and excreta that are key to K homeostasis (e.g. plasma, muscle, liver, kidney, urine). This consistency is likely owed to the conserved K metabolism across endothermic vertebrates, being at cellular or whole-body levels.[9–11,38,39,41] We consider thereafter the shared features in endothermic vertebrates to decipher the controls of K isotopes cycling in relation with K homeostasis.

Cellular cycling of K isotopes

The documented isotopic variability in tissues constitutive of the organism reveals the cellular mechanisms at play in the internal cycling of K isotopes.

Extracellular/intracellular isotopic dichotomy

Potassium cycling in cells is primarily characterized by the acute and actively maintained transmembrane concentration gradients.[9] This chemical gradient is paralleled by a net fractionation of K isotopes leading to the ^{41}K-enrichment of intracellular reservoirs (skeletal and cardiac muscles, liver, RBC) when compared to external fluids (plasma). Indeed, all strict intracellular reservoirs are markedly and significantly ^{41}K-enriched in comparison with extracellular K (Fig. 5A): $\Delta^{41}K_{Muscle}$ of ICF are higher than plasma by 0.52 ± 0.09‰ ($\Delta^{41}K_{Muscle}$, W: $P^{***} < 10^{-4}$, WMW: $P^{***} < 10^{-4}$, $n = 110$) with no overlap in the distributions.

A similar trend is observed in reservoirs that are not strictly representative of intracellular K. Bulk bone, which contains a mix of intracellular as well as organo-mineral bound K, is

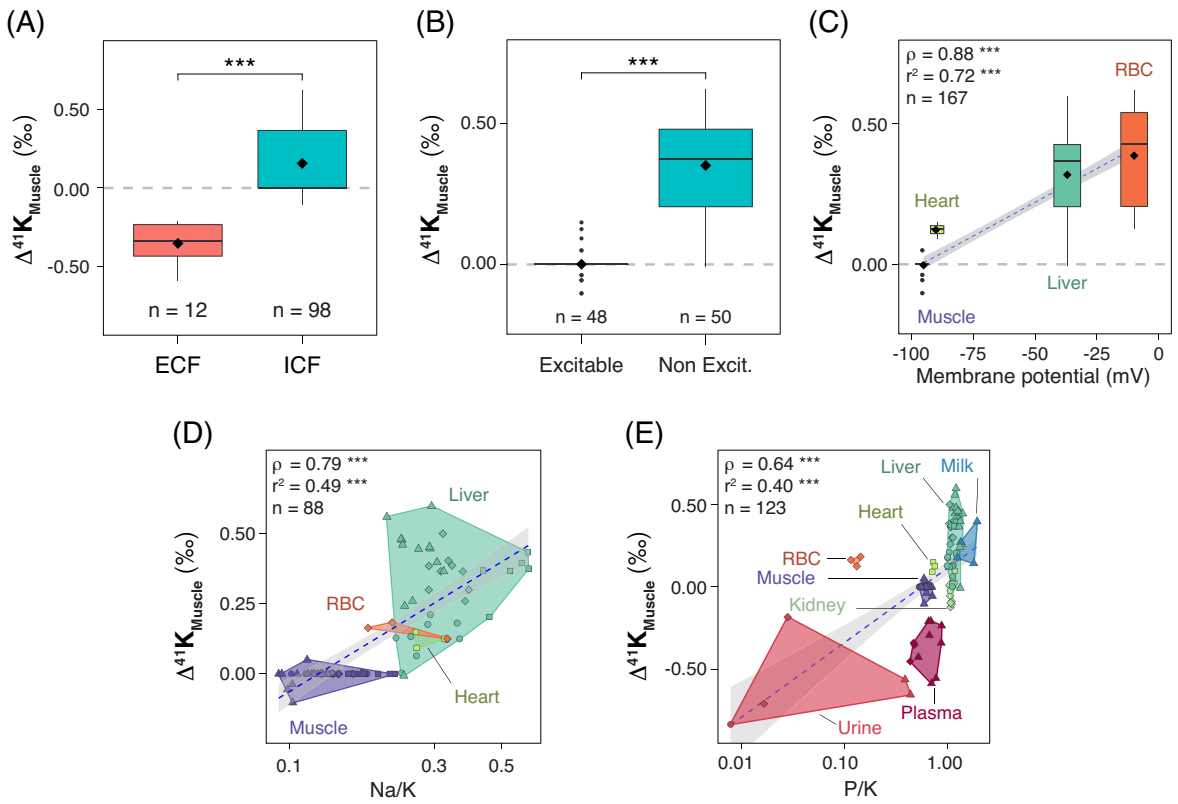

Fig. 5 Distributions of $\Delta^{41}K_{Muscle}$ values (A) in extracellular (blood plasma) and intracellular reservoirs (skeletal and cardiac muscle, liver, red blood cells) (W: $P^{***} < 10^{-4}$, WMW: $P^{***} < 10^{-4}$), (B) in excitable tissues (skeletal and cardiac muscle) and nonexcitable tissues (liver, red blood cells), (W: $P^{***} < 10^{-4}$, WMW: $P^{***} < 10^{-4}$, (C) in intracellular reservoirs plotted as a function of the typical resting membrane potential expressed in mV, values compiled from literature,[79–82] (D) in intracellular reservoirs against the Na/K concentrations ratios and (E) in all soft tissues and excreta against P/K concentrations ratios, as measured in this study.

overall heavier than plasma by 0.57 ± 0.15‰. Likewise, the kidney, which is ^{41}K-enriched by 0.34 ± 0.09‰, contains both intracellular and luminal K from primary urine. Despite these heterogeneous K pools, we can assume that the isotope compositions of these reservoirs are dominated by ICF K, as ICF concentrations are typically 20–40 times higher than in ECF or primary urine.[9] The ^{41}K-enrichment reported for these tissues is therefore also likely related to the ICF–ECF systematic difference while its extent is not directly comparable.

While all K reservoirs are not represented in the current dataset (e.g. brain), the magnitude and ubiquity of the ^{41}K-enrichment in intracellular reservoirs is remarkable and systematic: all aforementioned ICF K reservoirs represent ca. 86% of the whole-body K and ca. 87% of total ICF K (Supplementary Table SC13[40]). In this near total pool, a simple mass balance calculation points to a mean δ^{41}K of +0.5‰ to +0.6‰ higher than diet, or +0.4‰ higher than plasma.

This remarkable net isotope fractionation constitutes a salient trait of K isotope systematics in vertebrates. Such a dichotomy parallels the vital, maintained, and regulated K transmembrane concentration gradients shared by all vertebrate cells.[9,38,41] This suggests that the cellular and molecular mechanisms responsible for the intracellular ^{41}K-enrichment is widely shared and likely deeply rooted in the phylogeny of vertebrates.

These observations also show that K isotopes bear potential for the reconstruction of trophic relationships in vertebrate ecosystems. Indeed, as soft tissues are ^{41}K-enriched when compared to diet by ca. +0.5‰, the consumption of plants by herbivores and soft tissues by secondary and tertiary consumers (carnivores) will result in the propagation of this 0.5‰ offset up trophic chains. The use of K isotopes could hence complement other isotopic trophic markers (e.g.[7,8]). Moreover, because C3 and C4 plants appear to display markedly distinct isotope compositions,[83] K isotopes are likely to offer a synthetic description of the trophic structures of vertebrate tropical ecosystems, both for vegetal ecology and carnivory.

Cell homeostasis controls isotope fractionation

The understanding of the mechanisms leading to the ICF/ECF dichotomy will help to constrain the potential of K isotopes in vertebrate biology. Two types of nonmutually exclusive mechanisms can be proposed for the systematic ^{41}K-enrichment of ICF: (i) a preferential ^{41}K-influx upon inward transmembrane transport, or (ii) a preferential ^{39}K-efflux, upon outward transport or intracellular ^{41}K-retention.

The active pumping of K into the cytoplasm is mediated by the action of the ubiquitous NKA pump.[84–86] The passive efflux of K occurs down its electrochemical gradient through K-specific channels of various classes, all sharing the same pore-domain responsible for K transport.[87] Overall, both NKA and K-channel transport mechanisms involve partial to complete dehydration of K^+ ions, which at this point are mostly coordinated with oxygen from side and main chains binding sites.[84,87,88] Although the complexity of these mechanisms hinders any precise predictions, it is worth noticing that channels conduct K at near diffusion-limited rates, suggesting the involvement of weak interactions only.[87] This

would support a kinetic control over isotope fractionation, possibly favoring ^{39}K-efflux (e.g. Mahan *et al.*[4]). On the other hand, the saturable NKA involves an occlusive and likely stiffer binding of K, which would favor thermodynamic effects putatively leading to ^{41}K-influx. Finally, K processing in the cytoplasm or organelles could favor the thermodynamically controlled ^{41}K-retention due to intracellular counter-ions.[39,89] Although, the identification of biochemical mechanisms requires dedicated research,[45,90] the tissue-specific intracellular distributions of K isotopes bring valuable constraints because K cellular cycling is known to depend on cell types.

Our dataset shows that K cellular homeostasis and membrane permeability are central in the determination of intracellular K isotope compositions: the extent of ICF ^{41}K-enrichment appears to depend on cell excitability. As shown in Fig. 5B, nonexcitable cells (hepatocytes and RBC) are markedly ^{41}K-enriched relative to excitable cells (skeletal and cardiac myocytes) by 0.33 ± 0.05‰ ($\Delta^{41}K_{Muscle}$ scale, W: $P^{***} < 10^{-4}$, WMW: $P^{***} < 10^{-4}$, $n = 98$). The permeability of cell membranes to K is central to cell excitability. Indeed, the passive efflux of K in resting cells contributes ca. 90% of the RMP in most cells, typically ranging from −100 to −50 mV[9,86] and these values depend on cell excitability. Excitable cells (e.g. myocytes) typically display high K permeability responsible for strong polarization (RMP of −100 to −70 mV), while nonexcitable cells are less permeable to K and have less negative RMPs (−40 to −10 mV). The intensity of K cycling is therefore higher in resting excitable vs. nonexcitable tissue. Additionally, cycles of membrane depolarization/repolarization in excitable cells imply a higher K cellular turnover.[9] The isotopic differences between excitable and nonexcitable cells thus points to a key role of membrane permeability and intensity of K cellular cycling in the determination of intracellular ^{41}K-enrichment.

Furthermore, K membrane permeability is known to depend on tissues, which is reflected in the values of their RMPs. We conducted a first comparison of the $\Delta^{41}K_{Muscle}$ distributions of ICF reservoirs with their typical RMP values (Fig. 5C). Overall, we report a significant positive linear correlation between $\Delta^{41}K_{Muscle}$ and RMP of intracellular reservoirs. The ^{41}K-enrichment of the other intracellular reservoirs increases with RMP in a systematic manner from skeletal muscle to RBC. Although preliminary, these observations further support a negative link between the intensity of K cycling at the scale of the cell and the extent of ICF ^{41}K-enrichment. In other words, the tissue-specific distributions of K isotopes appear to reflect the electrical properties of cell membranes, and the more intense the K cellular cycling is, the less ^{41}K-enriched are the intracellular compartments.

The elemental distributions of K normalized to P and other essential cations (Na, Mg, Ca) further demonstrate the cell-specific homeostatic controls over K isotope distributions (Supplementary Fig. SB9). While we observe no significant links with Ca and Mg, which are not directly involved in K metabolism, K isotope compositions display clear links with Na/K and P/K ratios. Intracellular $\Delta^{41}K_{Muscle}$ is indeed strongly and positively correlated to Na/K (Fig. 5D). Tissues with low Na/K, representative of strong Na-K transmembrane opposite gradients and typical of excitable tissues (e.g. muscle), are not as ^{41}K-enriched as nonexcitable tissues, characterized by higher Na/K ratios (e.g. liver). This further supports that intracellular K isotope compositions are dependent on cell-specific K homeostasis, opposed by its Na antagonist. The $\Delta^{41}K_{Muscle}$ values are also positively and strongly correlated to P/K in strict intracellular reservoirs (Supplementary Fig. SB9) and more generally in soft tissues and excreta (Fig. 5E). With the exception of RBC (which lack respiratory metabolism and contain less ATP and total P[91–94]), the bulk P content of tissues is predominantly representative of organic bound phosphate as well as intracellular inorganic phosphate, which is ca. 19 times more concentrated in ICF than in ECF.[94] Bulk P in tissues can thus be considered a dry mass estimate relevant for intracellular K normalization. The significant correlation between $\Delta^{41}K_{Muscle}$ and P/K suggest that the extent of intracellular ^{41}K-enrichment is inversely correlated to ICF K concentrations. The smaller the intracellular K pool is, the more ^{41}K-enriched it is.

To summarize, the systematic ^{41}K-enrichment of cells is controlled by effectors of cellular homeostasis. This is manifested by the strong links with membrane K permeability and with the coupled homeostatic behaviors of Na and K. The amplitude of cell ^{41}K-enrichments is inversely related to the intensity of K cellular cycling and to the size of the intracellular K pool. This suggests a possible Rayleigh-type isotope distillation mechanism whereby the fractional loss of K from the intracellular milieu to the plasma induces a cumulative isotope effect amplified in smaller pools of "residual" intracellular K. Such a mechanism would be compatible with a preferential loss of light K isotopes upon efflux, because of facilitated ^{39}K-diffusion through K channels and/or a preferential intracellular ^{41}K-retention. This interpretation is in line with the conclusions of Higgins *et al.*[31] suggesting that the passive efflux of K through K-specific channels favors the loss of ^{39}K while active NKA influx induces no sizeable isotope fractionation.

Internal homeostasis controls of K isotopes cycle

The effectors of cellular K homeostasis are more generally those regulating the balance between intra- and extracellular K and define the internal homeostatic system.[9] This regulation system primarily relies on the control of intracellular stores of K in muscle and liver, and secondary reservoirs such as RBC.[10,11,39,86] The internal homeostasis therefore likely controls the distribution of K isotopes across bodily reservoirs, in health or disease. Transient net efflux or influx of intracellular K—as in intense physical exercise[86]—would then produce positive or negative excursions of δ^{41}K in the small pool of plasma K, respectively.

More generally, pathological organ or systemic disruptions of internal homeostasis have thus the potential to produce sizeable departures of the isotope compositions in blood plasma and all connected reservoirs. Temporary or chronic conditions affecting K cellular and hence internal homeostasis, either documented or yet to be described, are likely to affect the isotope balance between K reservoirs. A series of pathological conditions are known to be associated with impaired internal or cell K homeostasis and could be associated with modified K isotope distributions.[10] Furthermore, K isotopes could help finely track so far undetected alterations of cell K homeostases, in diseases such as cancer suspected to affect membrane resting potential and permeability.[95] In this context, K bears a great potential for the dynamic characterization of impaired cellular and internal K homeostasis, being for fundamental physiopathology or clinical applications.

Whole-body K isotopes cycling

Potassium internal homeostasis is functionally dependent on the external homeostatic system responsible for the regulation of the whole-body balance between K inputs and losses.[10,11,39] The controls of external homeostasis over the cycle of K isotopes are documented by the current dataset, allowing to propose a first model of the whole-body K isotope cycling.

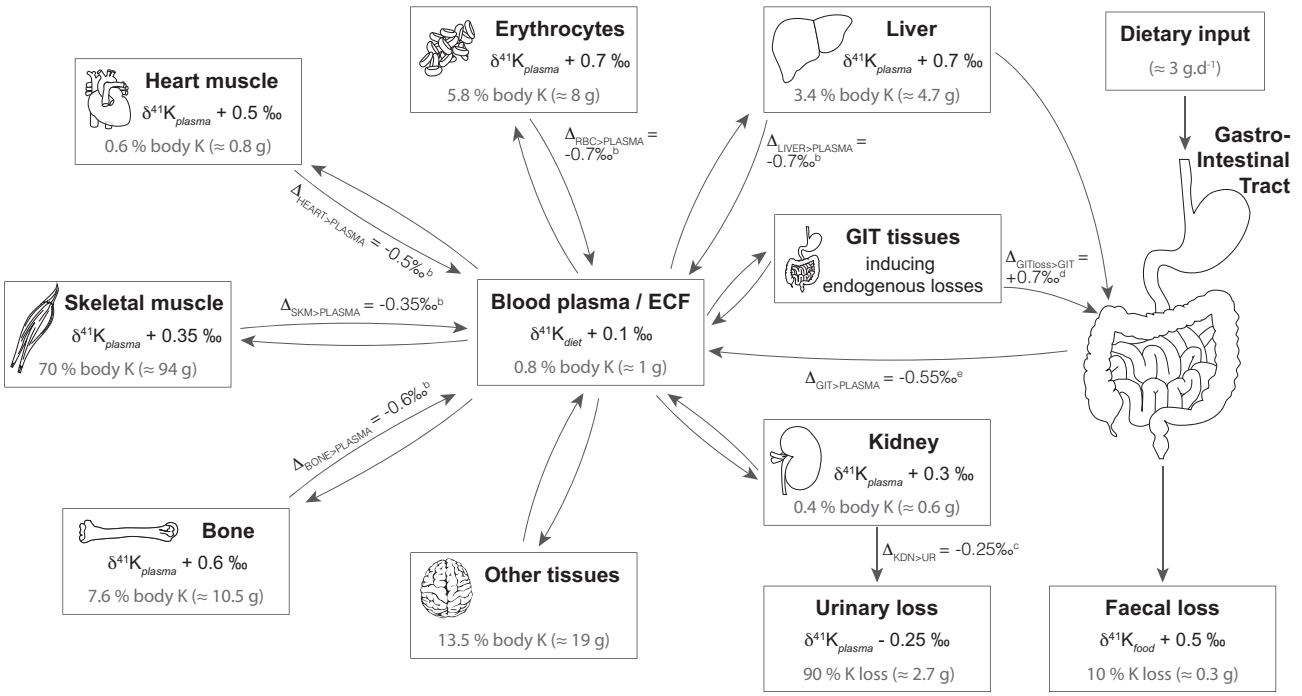

Fig. 6 Model of the cycle of K and its isotopes in endothermic vertebrates. Absolute K amounts (in g) are shown for an adult 70 kg human.[9,38,40,44] The typical isotope compositions of reservoirs are shown relative to the relevant reservoirs. The cycle was used in isotope box modeling with the various isotope fractionation hypotheses b–e presented in Table 3. The documented or likely isotope fractionation upon K transport is shown along the corresponding fluxes as Δ values and the corresponding fractionation hypothesis as superscript.

Transepithelial controls of isotope fractionation

The external homeostasis relies on the action of epithelia exchanging K with the exterior environment: the intestinal epithelium, allowing K absorption, but most importantly the regulated renal excretion in the distal nephron.[10,38] Transepithelial transport of K includes both (i) active transcellular pathways, involving the transmembrane protein transporters, and (ii) passive paracellular transport, via tight junctions selectively permeable to K.[10] Any net isotope fractionation occurring upon transepithelial transport of K could affect the baseline isotope composition of the system, starting with plasma central reservoir. The characterization of isotope effects induced by epithelia is thus critical.

It is shown here that the transfer of K across epithelia induces sizeable fractionation of K isotopes, as directly reported in two occurrences: (i) the excretion of urine in the renal epithelium and (ii) the production of milk in mammary glands, both resulting from transcellular transport mainly.[9,10,96,97]

First, urinary losses are significantly ^{41}K-depleted when compared to plasma, from which urinary K is derived, by −0.18 ± 0.17‰ on the $\Delta^{41}K_{Diet}$ scale (W: $P^* = 0.04$, WMW: $P = 0.07$, $n = 19$) and −0.29 ± 0.21‰ on the $\Delta^{41}K_{Muscle}$ scale (W: $P^* = 0.0125$, WMW: $P^* = 0.0130$). The renal excretion of K through the renal epithelium is therefore responsible for a fractionation of −0.2 to −0.3‰. Urinary K essentially results from K secretion in the distal tubule of the nephron because the quasi totality of K from the glomerular filtrate is actively reabsorbed in the proximal tubule.[10] As a result, the preferential loss of ^{39}K via kidneys results from the excretion of K in the distal tubules primarily upon transcellular transport. This observation completes the renal isotope fractionation described in rat by Higgins *et al.*, their results suggesting a slightly more pronounced isotope effect of the order of −0.5‰.[31]

Second, milk excretion in pigs induces a significant ^{41}K-enrichment with respect to plasma, by 0.69 ± 0.29‰ on the $\Delta^{41}K_{Diet}$ scale (W: P^{***}=0.0014, WMW: P^{**}=0.003, n = 13) and 0.59 ± 0.17‰ in $\Delta^{41}K_{Muscle}$ (W: P^{***}=0.0001, WMW: P^{**}=0.003). The exocrine excretion of K by mammary glands thus induces a transepithelial fractionation of the order of +0.7‰. The excretion of K by mammary glands is thought to occur primarily along transcellular pathways as well.[96,97] However, milk secretion produces a sizeable preferential loss of ^{41}K. This appears to contradict the trend described for urinary secretion. A possible explanation could lie in the central role of exocytosis in mammary gland exocrine functions, allowing the excretion of key milk components such as proteins or lipids.[96,97] The associated flux of K remains to be assessed but could cause a preferential loss of ^{41}K owing to subcellular cycling of K isotopes.

Finally, the transport of K across the epithelia of the GIT, either inward (absorption) or outward (endogenous losses), could also produce a sizeable isotope fractionation. However, these effects can only be here indirectly assessed based on feces isotope compositions, as discussed thereafter.

Systemic isotope homeostasis model

The implication of the effectors of external homeostasis (kidney, intestine, among others) in the determination of the whole-body K isotope distribution can be estimated and modeled based on mass balance considerations. This is done here using isotope box modeling. The typical K cycle in vertebrates is shown in Fig. 6 scaled for a human adult.[9,38,40,44] About 94% of K from diet is absorbed to plasma in the intestine. Around 95% of absorbed K is excreted in urine while the remaining fraction is lost to the digestive tract as endogenous losses. This includes digestive secretions from exocrine glands as well as cells shedding from

Table 3. Hypotheses (a to e) of isotope fractionation upon K transport[a]

Fractionation amplitudes	Fractionation hypotheses (as Δ values, ‰)				
Δ, *in ‰*	a No fractionation	b ^{39}K efflux	c Renal excretion	d Endogen. losses	e Intestinal absorption
$\Delta_{BONE>PLASMA}$	-	−0.57	−0.57	−0.57	−0.57
$\Delta_{HEART>PLASMA}$	-	−0.47	−0.47	−0.47	−0.47
$\Delta_{LIVER>PLASMA}$	-	−0.67	−0.67	−0.67	−0.67
$\Delta_{RBC>PLASMA}$	-	−0.74	−0.74	−0.74	−0.74
$\Delta_{SKM>PLASMA}$	-	−0.35	−0.35	−0.35	−0.35
$\Delta_{KDN>UR}$	-	-	−0.25	−0.25	−0.25
$\Delta_{GITloss>GIT}$	-	-	-	0.7	0.7
$\Delta_{GIT>PLASMA}$	-	-	-	-	−0.55

[a]Amplitudes of fractionation are shown as $\Delta_{i>j}$ values (in ‰), where $\Delta_{i>j} = \delta^{41}K_j - \delta^{41}K_i$ for boxes j and i. The conversion to fractionation factors ($\alpha_{i>j}$) is calculated as follows: $\alpha_{i>j} = \exp(\Delta_{i>j}/1000)$.

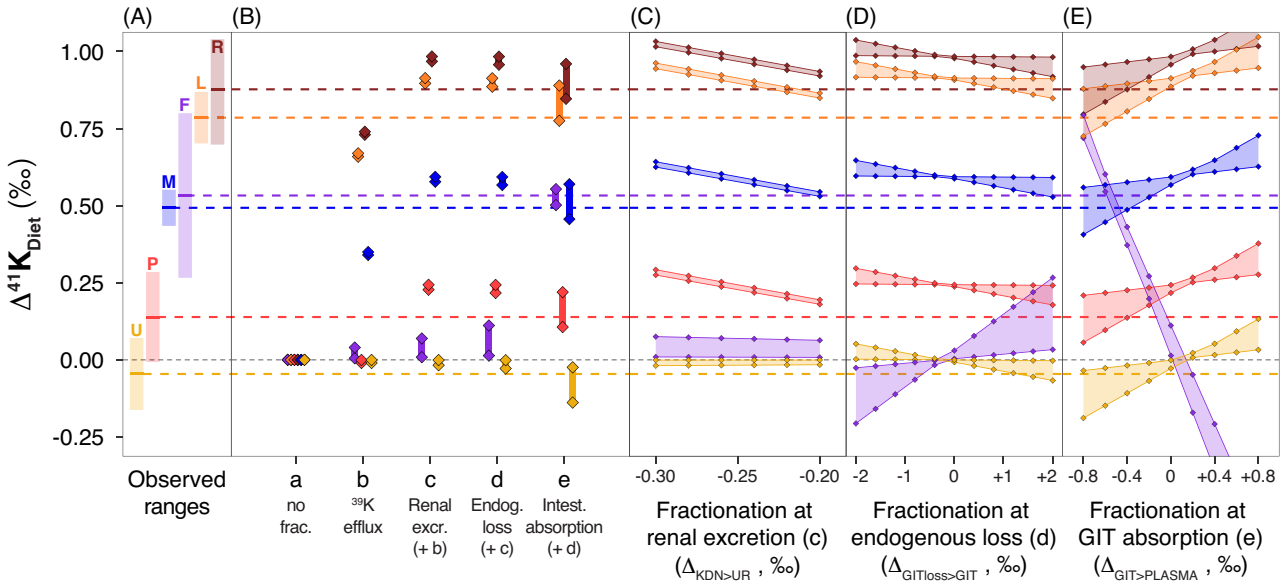

Fig. 7 $\Delta^{41}K_{Diet}$ results of the steady-state isotope box-model simulations for a subset of key K boxes. A: observed variability (mean line and 95% C.I. shaded area; U: urine, P: plasma, M: muscle, F: feces, L: liver, R: RBC); B: steady-state simulations in hypotheses a–e of isotope fractionations. Hypothesis a is shown as a reference for the absence of isotope fractionation; C: in the hypothesis c, i.e. preferential cellular ^{39}K efflux, with varying net fractionation at renal excretion; D: in the hypothesis d with varying net fractionation at endogenous losses; E: in the hypothesis e with varying net fractionation at intestinal absorption. The diamonds and associated vertical lines (B) or shaded area (C, D) show the full variability across all simulated flux configurations encompassing natural variability of K cycles. These results are also shown as $\Delta^{41}K_{Muscle}$ in Supplementary Fig. SB10.

GIT epithelia.[98] Endogenous losses typically account for a third of bulk fecal losses, the remainder corresponding to unabsorbed dietary K. Overall, 90% of dietary K is lost to urine against 10% in feces.[40,44]

Following ingestion and digestion, plasma plays the role of a central reservoir exchanging K with all other tissues and is the first to receive dietary K. Its baseline isotope composition is thus expected to ultimately determine those of downstream reservoirs. Plasma seems to be slightly ^{41}K-enriched relatively to diet, by 0.14 ± 0.15‰ (o.s. *t*-test: $P = 0.06$, $n = 12$) as measured in rats and pigs. When considering pigs only, which are fully equilibrated with their diets, plasma is significantly ^{41}K-enriched, by 0.17 ± 0.14‰ on average (o.s. *t*-test: $P^{**} = 0.009$, $n = 9$). Such a positive offset demonstrates a net isotope fractionation resulting in plasma ^{41}K-enrichment. Mass conservation laws dictate that the balanced exchange of plasma K with any other internal reservoir does not affect steady-state plasma composition. The ^{41}K-enrichment of plasma is hence induced by the preferential uptake of ^{41}K and/or loss of ^{39}K occurring across epithelia.

We tested the effects of the isotope effects discussed in the present study by comparing the observed K isotope distributions with the box-model outputs obtained using isotope fractionation hypotheses summarized in Table 3. The resulting simulations are shown as $\Delta^{41}K_{Diet}$ in Fig. 7 together with the observed compositions of key boxes.

As a starting hypothesis, we simulated the effects of fractionation between intracellular and extracellular K characterized earlier. Here, the amplitudes of the tissue specific isotope fractionation upon K efflux ($\Delta_{ICF > PLASMA}$) are set to the opposite amplitude of their documented ^{41}K-enrichment (Table 3, hypothesis b). The alternative hypothesis (^{41}K-influx) produces the same steady-state distributions and thus does not change the outcome of this discussion. As expected, these simulations reproduce the systematic ^{41}K-enrichment of intracellular reservoirs relative to

plasma (Fig. 7B). However, hypothesis b fails to reproduce realistic $\Delta^{41}K_{Diet}$ of intracellular reservoirs as well as feces, which remain far below their observed ranges. Furthermore, plasma and urine fall at 0‰, contradicting the documented ^{41}K-enrichment of plasma relative to diet and urine.

A ^{41}K-enrichment of plasma with respect to diet could derive from a preferential loss of lighter K. As most absorbed K is lost in urine (ca. 95%), renal excretion could be responsible for plasma ^{41}K-enriched values. The renal isotope effect is tested by forcing a preferential loss of ^{39}K upon urine excretion varying from −0.3 to −0.2‰ (Fig. 7C). While urine is only slightly ^{41}K-depleted and stays in line with observed ranges, the renal isotope effect produces realistic ^{41}K-enriched plasma compositions, by 0.19–0.29‰ with respect to diet. This effect is also propagating to all ICF reservoirs (muscle, liver, RBC), which are shifted within or close to the higher end of their documented variability. Such a sizeable effect on plasma is expected because urinary losses represent most total losses. Additionally, these results hold irrespective of the variations of simulated K cycles, covering highly variable balances in urinary vs. endogenous losses (85–97% vs. 3–15% of absorbed K, respectively, Appendix A, Text A.1., Section A.1.2.). While urinary losses are reported to be higher than 95% of absorbed K,[44] even lower yet less realistic urinary losses (down to 85%) do not produce any sizeable differences in these distributions. This is summarized in hypothesis c, assuming an intermediate −0.25‰ renal effect (Fig. 7B, hyp. c).

Overall, the renal effect alone is sufficient to reproduce the plasma ^{41}K-enrichment and the diet-like composition of urine as well as realistic compositions of intracellular reservoirs, although systematically on the higher end of their documented variability. The kidney function thus drives the baseline isotope composition of the organism. However, this effect alone fails to reproduce the composition of feces, which remain near 0‰, i.e. far below their observed compositions.

The GIT represents another major interface in K homeostasis. The current dataset does not allow to directly assess the direction and extent of any isotope fractionation upon entry (intestinal absorption) or outflow (endogenous losses) across the GIT epithelia. While the previous hypotheses (a to c) fail to reproduce the documented ^{41}K-enriched compositions of fecal K, feces represent the only source of information at hand to infer the roles of the digestive K physiology on the isotope homeostasis. Although variable across pigs and guinea pigs, feces are overall significantly ^{41}K-enriched with respect to diet, by 0.53 ± 0.27‰ on average. Such a sizeable ^{41}K-enrichment could result from the preferential loss of endogenous ^{41}K and/or a preferential intestinal ^{39}K absorption.

The effect of a putative isotope fractionation upon endogenous losses was first assessed by forcing a net isotope fractionation ranging from −2 to+2‰ at all endogenous losses pooled together (bile and other losses, Fig. 7D). The results show that the only way to produce realistic feces $\Delta^{41}K_{Diet}$ would be to assume a net isotope fractionation of +2‰ or more. However, this remains unlikely because: (i) the extent of such a net isotope effect at endogenous losses appears three times as high as the maximum documented transepithelial isotope effect (+0.7‰ in milk, −0.3‰ in urine), (ii) the highest simulated feces $\Delta^{41}K_{Diet}$ values (up to +0.25‰) are only explained with more than 70% endogenous K in total feces, while this values is reported to actually lie around 30–40%,[44] (iii) nevertheless assuming these assumptions hold true, the extent of feces ^{41}K-enrichment remains below the lower end of the observed compositions of feces. As a result, while endogenous losses likely contribute ^{41}K to bulk feces to some extent, they hardly explain the observed distributions of K isotopes in the organisms, especially in feces.

As a consequence, although endogenous losses do not explain feces compositions, we set the isotope fractionation upon transfer from plasma to GIT at +0.7‰ (hyp.d, $\Delta_{GITloss>GIT}$, c.f. Table 3) for several reasons. Endogenous losses are partly dependent on K excretion by digestive exocrine glands, and the isotope composition of milk, also produced by an exocrine gland, is ^{41}K-enriched relative to plasma by about +0.7‰. The shedding of digestive epithelial cells also contributes to the K endogenous losses, and we can assume that the isotope composition of intracellular K of epithelial cells compares to that of other nonexcitable tissues, lying ca. +0.7‰ higher than plasma. Finally, bile secreted by liver also contributes K to endogenous losses. We assume that bile contributes half of endogenous K and we do not force any isotope fractionation upon bile secretion. This leaves bile at the same isotope composition as liver, i.e. +0.7‰ higher than blood plasma. The simulations (Fig. 7B, hyp. d) show that the effects of such a fractionation at the loss of endogenous K to the GIT remain limited: predicted feces $\Delta^{41}K_{Diet}$ remains near 0‰ or slightly positive, and far below the reported compositions. We also note that the other reservoirs appear to remain unchanged.

Alternatively, feces ^{41}K-enrichment could derive from a preferential ^{39}K uptake at intestinal absorption. In the hypothesis of a preferential intestinal ^{39}K-uptake, we expect the minor pool of unabsorbed K (≈6% of dietary K) to be strongly enriched in ^{41}K with respect to initial diet, while the major pool of absorbed K (≈94%) would tend to be moderately ^{41}K-depleted. To explore the effects of intestinal absorption isotope effects in addition to previous hypotheses (b, c, and d), we let the isotope fractionation upon GIT absorption vary between −0.8 and+0.8‰ (Fig. 7E). The simulations show that fecal K is highly dependent on the absorption effect while we observe little dependence on the variable K flux configurations. A preferential intestinal ^{41}K-uptake ($\Delta_{GIT>PLASMA} > 0$‰) produces unrealistic compositions for feces and for the other reservoirs to a lesser extent. Alternatively, the preferential uptake of ^{39}K from digesta ($\Delta_{GIT>PLASMA} < 0$‰) easily produces realistic feces values for a $\Delta_{GIT>PLASMA}$ between −0.8 and −0.3‰. Moreover, such an absorption effect tends to lower the $\Delta^{41}K_{Diet}$ of plasma and of all downstream reservoirs within their range of observed variability and towards their documented average compositions. As a consequence, we conclude that the fractionation at intestinal absorption lies around the middle point of that range, i.e. ca. −0.55‰. The order of magnitude of such an isotope effect upon K transepithelial transport seems realistic, as its extent resembles those of other directly measured transepithelial isotope effects (e.g. milk or urine excretion). Moreover, paracellular pathways were reported for K absorption in some sections of the small intestine (ileum, jejunum, colon[39,99]). Such passive transport mechanisms could induce diffusion-controlled isotope fractionation, putatively in favor of the transport of the light isotopes, assuming kinetic control. The simulated distributions produced by this model (Fig. 7B, hyp. e) are in remarkably good agreement with the mean compositions measured in these reservoirs. Finally, this conclusion corroborates the findings of Higgins *et al.*, who suggest that paracellular pathways favor the transport of light K isotopes.[31]

To conclude, we show that (i) K renal excretion likely drives the baseline isotope composition of blood plasma, (ii) the influence of endogenous losses in the GIT appears to be negligible both for whole body and fecal isotope compositions, and (iii) the intestinal

absorption of K is very likely responsible for a preferential uptake of ^{39}K, moderately affecting baseline internal compositions and primarily responsible for feces ^{41}K-enriched compositions.

These conclusions complete the characterization of the internal homeostatic controls and demonstrate that external homeostasis also controls K isotope distribution in the organism. Consequently, we can predict that transient or chronic disruptions of K external homeostasis affecting renal or intestinal functions for instance will translate into sizeable perturbations of K isotopic baselines. Potassium isotopes hence bear the potential to track systemic K imbalances in pathological contexts, being notoriously affecting K homeostasis (e.g. chronic kidney diseases[100]) or for which K dyshomeostasis remained cryptic until now. In the future, the roles of other secondary losses should be considered, such as integuments (e.g. skin, hair, perspiration[40,86]).

Conclusion

The biological processing of K by endothermic vertebrates produces sizeable and systematic fractionation of its isotopes in three mammalian and one avian species. Such a consistency indicates shared isotope fractionation mechanisms, reflecting the conserved K physiology across endothermic vertebrates.

The $\delta^{41}K$ values of vertebrate tissues are primarily determined by those of diet, while K of vertebrate soft tissues, found essentially in cellular compartments, are ^{41}K-enriched with respect to diet by ca. +0.5‰. In such a configuration, the consumption of plant by herbivores and animal tissues by carnivores is expected to result in the propagated +0.5‰ stepwise increase of vertebrate tissues $\delta^{41}K$ along food chains, hence defining so-called trophic level effects. For these reasons, K isotopes could constitute a new trophic biomarker in the toolbox of stable isotope paleobiology, relevant to questions in vertebrate ecology and evolution.[7,8] The calibration of such a novel biomarker would require further research in modern ecosystems, while the application to fossil settings should be accompanied by the assessment of the conservation potential of biogenic K isotope compositions in skeletal remains, such as tooth enamel.

Beyond the dietary controls, the cycling of K isotopes by endothermic vertebrates is strongly related to the homeostatic system, regulating K cycles from cells to the whole organism.

In cells, the systematic ^{41}K-enrichment of the cytoplasm is controlled by mechanisms involved in K cellular homeostasis. As a result, because the effectors of this homeostasis constitute the basis of internal homeostasis, K isotopes are expected to reflect physiological and pathological variations in the balance between intra- and extracellular K pools. Changes in health or in disease of K cellular cycling, or internal homeostasis, are hence likely to alter steady-state K isotope distributions, including in the small circulating pool of plasma K. For instance, the proliferation of tumoral cells, with altered membrane permeability to K, could affect plasma baseline $\delta^{41}K$.[95] Likewise, neurodegenerative diseases such as Alzheimer's disease are known to be associated with modified brain K distributions and NKA activity,[101] which could lead to modified intra- vs. extracellular distributions of K isotopes.

We show that transepithelial transports of K also produce sizeable isotope effects, hence controlling the baseline isotope composition of the organism. As epithelia, and especially kidneys, are the primary effectors of external homeostasis, changes of the K whole-body balance are expected to induce sizeable variations of isotope composition of the organism, starting with blood plasma. Given the central role of the kidney in K isotope homeostasis, a positive whole-body K balance is for instance expected to prompt negative shifts of plasma $\delta^{41}K$ values, and vice versa.

Overall, K isotopes show great potential in the field of isotope metallomics and promise to shed new light on the regulated or impaired cycling of K. The dependency of K isotope cycling to determinants of K homeostasis indicate that variations in bodily $\delta^{41}K$ document the status and dynamics of K cellular, internal, and external homeostasis. The use of K isotopes in easily sampled biofluids could thus help detect and characterize metabolic imbalances when approaches based on quantitative parameters like kalemia remain potentially insensitive (because such parameters are subject to homeostatic compensations even in disease). A K isotope biomarker would pave the way to new findings in the roles of K in fundamental physiology and pathology, as well as for the development of new generations of prognostic or diagnostic biomarkers.[1–5]

Supplementary material

Supplementary data are available at *Metallomics* online.

Acknowledgements

The authors wish to thank Daniela Winkler and Jennifer Leichliter for their advice and help in feeding experiment A sample collection. The authors are also thankful to Alan Stewart for running feeding experiment B. The authors also thank Nicholas S. Lloyd and Johannes B. Schwieters from Thermo Fisher Scientific in Bremen for their advice on Proteus. Finally, we thank two anonymous reviewers for their insightful comments that helped improve this manuscript.

Author contributions

T.Ta. designed the study. M.C. and T.Tü. designed feeding experiment A. R.E. designed feeding experiment B. T.Ta., M.C., T.Tü., J.L. and R.E. contributed to sample collection. T.Ta., J.L., C.D.C., TRE developed the analytical procedures for K isotope analyses. T.Ta. performed K. isotope analyses. T.Ta. and E.A. performed elemental analyses. TTa evaluated the data, ran numerical simulations, and wrote the original draft. All authors contributed to discussion and editing of the final manuscript.

Funding

This article is part of the BioIsoK project that has received funding from the European Union's Horizon 2020 research and innovation programme under the Marie Skłodowska-Curie grant agreement number 798583 BIOISOK IEF. The feeding experiment A (rats, guinea pigs, quails) received funding from the European Research Council (ERC) under the European Union's Horizon 2020 research and innovation programme, grant agreement no. 681450. The development of the Proteus prototype received funding from the ERC Advanced Grant 321209 "ISONEB."

Conflicts of interest

The authors declare no conflicts of interest.

Data availability

The data underlying this article are available in the article and in its online supplementary material.

References

1. F. Albarède, Metal Stable Isotopes in the Human Body: a Tribute of Geochemistry to Medicine, *Elements*, 2015, 11 (4), 265–269. https://doi.org/10.2113/gselements.11.4.265
2. M. Costas-Rodríguez, J. Delanghe and F. Vanhaecke, High-Precision Isotopic Analysis of Essential Mineral Elements in Biomedicine: Natural Isotope Ratio Variations as Potential Diagnostic and/or Prognostic Markers, *Trends Anal. Chem.*, 2016, 76, 182–193. https://doi.org/10.1016/j.trac.2015.10.008
3. T. Tacail, S. Le Houedec and J. L. Skulan, New Frontiers in Calcium Stable Isotope Geochemistry: Perspectives in Present and Past Vertebrate Biology, *Chem. Geol.*, 2020, 537, 119471 https://doi.org/10.1016/j.chemgeo.2020.119471
4. B. Mahan, R. S. Chung, D. L. Pountney, F. Moynier and S. Turner, Isotope Metallomics Approaches for Medical Research, *Cell. Mol. Life Sci.*, 2020, 77 (17), 3293–3309. https://doi.org/10.1007/s00018-020-03484-0.
5. F. Albarède, P. Télouk, V. Balter, V. P. Bondanese, E. Albalat, P. Oger, P. Bonaventura, P. Miossec and T. Fujii, Medical Applications of Cu, Zn, and S Isotope Effects, *Metallomics*, 2016, 8 (10), 1056–1070. https://doi.org/10.1039/C5MT00316D.
6. K. Jaouen and M.-L. Pons, Potential of Non-Traditional Isotope Studies for Bioarchaeology, *Archaeol. Anthropol. Sci.*, 2016, 9 (7), 1389–1404. https://doi.org/10.1007/s12520-016-0426-9.
7. J. E. Martin, T. Tacail and V. Balter, Non-Traditional Isotope Perspectives in Vertebrate Palaeobiology, Smith A (ed.). *Palaeontology*, 2017, 60 (4), 485–502. https://doi.org/10.1111/pala.12300
8. K. Jaouen, What Is Our Toolbox of Analytical Chemistry for Exploring Ancient Hominin Diets in the Absence of Organic Preservation?, *Quat. Sci. Rev.*, 2018, 197, 307–318. https://doi.org/10.1016/j.quascirev.2018.07.042.
9. M. J. V. Clausen and H. Poulsen, Sodium/Potassium Homeostasis in the Cell, In: L Banci (ed.). *Metallomics and the Cell*. Vol 12. Dordrecht, Netherlands: Springer Netherlands, 2013, 41–67.
10. B. F. Palmer and D. J. Clegg, Physiology and Pathophysiology of Potassium Homeostasis: Core Curriculum 2019, *Am. J. Kidney Dis.*, 2019, 74 (5), 682–695. https://doi.org/10.1053/j.ajkd.2019.03.427.
11. M. L. Gumz, L. Rabinowitz and C. S. Wingo, An Integrated View of Potassium Homeostasis, Ingelfinger JR (ed.). *N. Engl. J. Med.*, 2015, 373 (1), 60–72. https://doi.org/10.1056/NEJMra1313341.
12. M. Berglund and M. E. Wieser, Isotopic Compositions of the Elements 2009 (IUPAC Technical Report), *Pure Appl. Chem.*, 2011, 83 (2), 397–410. https://doi.org/10.1351/PAC-REP-10-06-02.
13. D. Wielandt and M. Bizzarro, A TIMS-Based Method for the High Precision Measurements of the Three-Isotope Potassium Composition of Small Samples, *J. Anal. At. Spectrom.*, 2011, 26 (2), 366. https://doi.org/10.1039/C0JA00067A.
14. C. D. Coath, T. Elliott and R. C. Hin, Double-Spike Inversion for Three-Isotope Systems, *Chem. Geol.*, 2017, 451, 78–89. https://doi.org/10.1016/j.chemgeo.2016.12.025.
15. Y. Hu, X. Y. Chen, Y. K. Xu and F. Z. Teng, High-Precision Analysis of Potassium Isotopes by HR-MC-ICPMS, *Chem. Geol.*, 2018, 493, 100–108. https://doi.org/10.1016/j.chemgeo.2018.05.033
16. L. E. Morgan, D. P. Santiago Ramos, B. Davidheiser-Kroll, J. Faithfull, N. S. Lloyd, R. M. Ellam and J. A. Higgins, High-Precision 41 K/39 K Measurements by MC-ICP-MS Indicate Terrestrial Variability of δ 41 K, *J. Anal. At. Spectrom.*, 2018, 33 (2), 175–186. https://doi.org/10.1039/C7JA00257B
17. K. Hobin, M. C. Rodríguez and F. Vanhaecke, Robust Potassium Isotopic Analysis of Geological and Biological Samples via Multicollector ICP-Mass Spectrometry Using the "Extra- High Resolution Mode," *Anal. Chem.*, 2021, 93 (25),8881–8888. https://doi.org/10.1021/acs.analchem.1c01087.
18. H. Chen, N. J. Saunders, M. Jerram and A. N. Halliday, High-Precision Potassium Isotopic Measurements by Collision Cell Equipped MC-ICPMS, *Chem. Geol.*, 2021, 578, 120281. https://doi.org/10.1016/j.chemgeo.2021.120281.
19. F. Moynier, Y. Hu, K. Wang, Y. Zhao, Y. Gérard, Z. Deng, J. Moureau, W. Li, J. I. Simon and F. Z. Teng, Potassium Isotopic Composition of Various Samples Using a Dual-Path Collision Cell-Capable Multiple-Collector Inductively Coupled Plasma Mass Spectrometer, Nu Instruments Sapphire, *Chem. Geol.*, 2021, 571, 120144. https://doi.org/10.1016/j.chemgeo.2021.120144.
20. K. Wang and S. B. Jacobsen, An Estimate of the Bulk Silicate Earth Potassium Isotopic Composition Based on MC-ICPMS Measurements of Basalts, *Geochim. Cosmochim. Acta*, 2016, 178, 223–232. https://doi.org/10.1016/j.gca.2015.12.039.
21. W. Li, B. Beard and S. Li, Precise Measurement of Stable Potassium Isotope Ratios Using A Single Focusing Collision Cell Multi-Collector ICP-MS, *J. Anal. At. Spectrom.*, 2016, 31 (4), 1023–1029. https://doi.org/10.1039/C5JA00487J.
22. D. P. Santiago Ramos, L. A. Coogan, J. G. Murphy and J. A. Higgins, Low-Temperature Oceanic Crust Alteration and the Isotopic Budgets of Potassium and Magnesium in Seawater, *Earth Planet. Sci. Lett.*, 2020, 541, 116290.
23. F. Z. Teng, Y. Hu, J. L. Ma, G. J. Wei and R. L. Rudnick, Potassium Isotope Fractionation during Continental Weathering and Implications for Global K Isotopic Balance, *Geochim. Cosmochim. Acta*, 2020, 278, 261–271. https://doi.org/10.1016/j.gca.2020.02.029.
24. T.-Y. Huang, F.-Z. Teng, R. L. Rudnick, X.-Y. Chen, Y. Hu, Y.-S. Liu and F.-Y. Wu, Heterogeneous Potassium Isotopic Composition of the Upper Continental Crust, *Geochim. Cosmochim. Acta*, 2019, 74, 6867–6884.
25. C. A. Parendo, S. B. Jacobsen and K. Wang, K Isotopes as a Tracer of Seafloor Hydrothermal Alteration, *Proc. Natl. Acad. Sci. U.S.A.*, 2017, 114 (8), 1827–1831. https://doi.org/10.1073/pnas.1609228114.
26. B. Tuller-Ross, B. Marty, H. Chen, K. A. Kelley, H. Lee and K. Wang, Potassium Isotope Systematics of Oceanic Basalts, *Geochim. Cosmochim. Acta*, 2019, 259, 144–154. https://doi.org/10.1016/j.gca.2019.06.001.
27. S. Li, W. Li, B. L. Beard, M. E. Raymo, X. Wang, Y. Chen and J. Chen, K Isotopes as a Tracer for Continental Weathering and Geological K Cycling, *Proc. Natl. Acad. Sci.*, 2019, 201811282.
28. D. P. Santiago Ramos, L. E. Morgan, N. S. Lloyd and J. A. Higgins, Reverse Weathering in Marine Sediments and the Geochemical Cycle of Potassium in Seawater: Insights from the K Isotopic Composition (41 K/39 K) of Deep-Sea Pore-Fluids, *Geochim. Cosmochim. Acta*, 2018, 236, 99–120. https://doi.org/10.1016/j.gca.2018.02.035.
29. K. Wang, W. Li, S. Li, Z. Tian, P. Koefoed and X.-Y. Zheng, Geochemistry and Cosmochemistry of Potassium Stable Isotopes, *Geochemistry*, 2021, 81 (3), 125786. https://doi.org/10.1016/j.chemer.2021.125786.
30. F. Moynier, Y. Hu, W. Dai, B. Mahan and J. MOUREAU, Potassium Isotopic Composition of 7 Widely Available Biological Standards Using Collision Cell (CC)-MC-ICP-MS, *J. Anal. At. Spectrom.*, 2021, 32 (11), 2444–2448. https://doi.org/10.1039/D1JA00294E.
31. J. A. Higgins, D. S. Ramos, S. Gili, C. Spetea, S. Kanoski, D. Ha, A. A. McDonough and J. H. Youn, Stable Potassium Isotopes (41 K/39 K) Track Transcellular and Paracellular Potassium

Transport in Biological Systems, *Front. Physiol.*, 2022, 13, 1–14. https://doi.org/10.3389/fphys.2022.1016242.
32. J. N. Christensen, L. Qin, S. T. Brown and D. J. DePaolo, Potassium and Calcium Isotopic Fractionation by Plants (Soybean [*Glycine max*], Rice [*Oryza sativa*], and Wheat [*Triticumaestivum*]), *ACS Earth Space Chem.*, 2018, 2 (7), 745–752. https://doi.org/10.1021/acsearthspacechem.8b00035.
33. W. Li, Vital Effects of K Isotope Fractionation in Organisms: Observations and a Hypothesis, *Acta Geochim.*, 2017, 214, 1–13. https://doi.org/10.1016/j.gca.2017.07.037.
34. W. Li, X. M. Liu, K. Wang, F. J. Fodrie, T. Yoshimura and Y. F. Hu, Potassium Phases and Isotopic Composition in Modern Marine Biogenic Carbonates, *Geochim. Cosmochim. Acta*, 2021, 304, 364–380. https://doi.org/10.1016/j.gca.2021.04.018.
35. K. Wang, H. G. Close, B. Tuller-Ross and H. Chen, Global Average Potassium Isotope Composition of Modern Seawater, *ACS Earth Space Chem.*, 2020, 4 (7), 1010–1017. https://doi.org/10.1021/acsearthspacechem.0c00047.
36. Y. Sun, F.-Z. Teng, Y. Hu, X.-Y. Chen and K.-N. Pang, Tracing-subducted Oceanic Slabs in the Mantle by Using Potassium Isotopes, *Geochim. Cosmochim. Acta*, 2020, 278, 353–360. https://doi.org/10.1016/j.gca.2019.05.013.
37. W. Li, X. M. Liu, Y. Hu, F. Z. Teng, Y. F. Hu and O. A. Chadwick, Potassium Isotopic Fractionation in a Humid and an Arid Soil—Plant System in Hawai'i, *Geoderma*, 2021, 400, 115219. https://doi.org/10.1016/j.geoderma.2021.115219.
38. J. H. Youn and A. a. McDonough, Recent Advances in Understanding Integrative Control of Potassium Homeostasis, *Annu. Rev. Physiol.*, 2009, 71 (1), 381–401. https://doi.org/10.1146/annurev.physiol.010908.163241.
39. D. Turck, J. L. Bresson, B. Burlingame, T. Dean, S. Fairweather-Tait, M. Heinonen, K. I. Hirsch-Ernst, I. Mangelsdorf, H. McArdle, M. Neuhäuser-Berthold, G. Nowicka, K. Pentieva, Y. Sanz, A. Siani, A. Sjödin, M. Stern, D. Tomé, H. Van Loveren, M. Vinceti, P. Willatts, P. Aggett, A. Martin, H. Przyrembel, A. Brönstrup, J. Ciok, J. A. Gómez Ruiz, A. de Sesmaisons-Lecarré and A. Naska, Dietary Reference Values for Potassium, *EFSA J.*, 2016, 14, e04592.
40. R. W. Leggett and L. R. Williams, A Model for the Kinetics of Potassium in Healthy Humans, *Phys. Med. Biol.*, 1986, 31 (1), 23–42. https://doi.org/10.1088/0031-9155/31/1/003.
41. P. W. Hochachka and G. N. Somero, *Biochemical Adaptation: Mechanism and Process in Physiological Evolution*. New York: Oxford University Press, 2002.
42. G. A. Morrill, A. B. Kostellow, L. Liu, R. K. Gupta and A. Askari, Evolution of the α-Subunit of Na/K-ATPase from Paramecium to Homo Sapiens: Invariance of Transmembrane Helix Topology, *J. Mol. Evol.*, 2016, 82 (4-5), 183–198. https://doi.org/10.1007/s00239-016-9732-1.
43. D. F. Rolfe and G. C. Brown, Cellular Energy Utilization and Molecular Origin of Standard Metabolic Rate in Mammals, *Physiol. Rev.*, 1997, 77 (3), 731–758. https://doi.org/10.1152/physrev.1997.77.3.731.
44. R. Agarwal, R. Afzalpurkar and J. S. Fordtran, Pathophysiology of Potassium Absorption and Secretion by the Human Intestine, *Gastroenterology*, 1994, 107 (2), 548–571. https://doi.org/10.1016/0016-5085(94)90184-8.
45. J. -. L. Cadiou, S. Pichat, V. P. Bondanese, A. Soulard, T. Fujii, F. Albarède and P. Oger, Copper Transporters Are Responsible for Copper Isotopic Fractionation in Eukaryotic Cells, *Sci. Rep.*, 2017, 7 (1), 44533. https://doi.org/10.1038/srep44533.
46. A. Heuser, *Biomedical Application of Ca Stable Isotopes. Calcium Stable Isotope Geochemistry*. Heidelberg, Germany: Springer Berlin, 2016, 247–260.
47. N. Gussone, G. Langer, S. Thoms, G. Nehrke, A. Eisenhauer, U. Riebesell and G. Wefer, Cellular Calcium Pathways and Isotope Fractionation in Emilianiahuxleyi, *Geol*, 2006, 34 (8), 625–628. https://doi.org/10.1130/G22733.1.
48. F. Böhm, N. Gussone, A. Eisenhauer, W. C. Dullo, S. Reynaud and A. Paytan, Calcium Isotope Fractionation in Modern Scleractinian Corals, *Geochim. Cosmochim. Acta*, 2006, 70 (17), 4452–4462. https://doi.org/10.1016/j.gca.2006.06.1546
49. E. Paredes, E. Avazeri, V. Malard, C. Vidaud, P. E. Reiller and R. Ortega, Evidence of Isotopic Fractionation of Natural Uranium in Cultured Human Cells, *Proc. Natl. Acad. Sci. U.S.A.*, 2016, 113 (49), 14007–14012. https://doi.org/10.1073/pnas.1610885113.
50. E. C. Webb, J. Lewis, A. Shain, E. Kastrisianaki-Guyton, N. V. Honch, A. Stewart, B. Miller, J. Tarlton and R. P. Evershed, The influence of Varying Proportions of Terrestrial and Marine Dietary Protein on the Stable Carbon-Isotope Compositions of Pig Tissues from a Controlled Feeding Experiment, *STAR Sci. Technol. Archaeol. Res.*, 2017, 3, 36–52.
51. J. N. Leichliter, T. Lüdecke, A. D. Foreman, N. N. Duprey, D. E. Winkler, E. R. Kast, H. Vonhof, D. M. Sigman, G. H. Haug, M. Clauss, T. Tütken and A. Martínez-García, Nitrogen Isotopes in Tooth Enamel Record Diet and Trophic Level Enrichment: Results from a Controlled Feeding Experiment, *Chem. Geol.*, 2021, 563, 120047. https://doi.org/10.1016/j.chemgeo.2020.120047
52. E. C. Webb, A. Stewart, B. Miller, J. Tarlton and R. P. Evershed, Age Effects and the Influence of Varying Proportions of Terrestrial and Marine Dietary Protein on the Stable Nitrogen-Isotope Compositions of Pig Bone Collagen and Soft Tissues from a Controlled Feeding Experiment, *STAR Sci. Technol. Archaeol. Res.*, 2016, 2, 54–66.
53. J. Lewis, A. W. G. Pike, C. D. Coath and R. P. Evershed, Strontium Concentration, Radiogenic (87 Sr/86 Sr) and Stable (δ 88 Sr) Strontium Isotope Systematics in a Controlled Feeding Study, *STAR Sci. Technol. Archaeol. Res.*, 2017, 3, 53–65.
54. I. Rosborg, *Drinking Water Minerals and Mineral Balance*. I Rosborg (ed.). Cham, Switzerland: Springer, 2015.
55. E. Albalat, P. Telouk, V. Balter, T. Fujii, V. P. Bondanese, M. Plissonnier, V. Vlaeminck-Guillem, J. Baccheta, N. Thiam, P. Miossec, F. Zoulim, A. Puisieux and F. Albarède, Sulfur Isotope Analysis by MC-ICP-MS and Application to Small Medical Samples, *J. Anal. At. Spectrom.*, 2016, 31 (4), 1002–1011. https://doi.org/10.1039/C5JA00489F.
56. L. Sauzéat, M. Costas-Rodríguez, E. Albalat, N. Mattielli, F. Vanhaecke and V. Balter, Inter-Comparison of Stable Iron, Copper and Zinc Isotopic Compositions in Six Reference Materials of Biological Origin, *Talanta*, 121576, 2021, 221, DOI: 10.1016/j.talanta.2020.121576. https://doi.org/10.1016/j.talanta.2020.121576.
57. M. Klaver, D. A. Ionov, E. Takazawa and T. Elliott, The Non-Chondritic Ni Isotope Composition of Earth's Mantle, *Geochim. Cosmochim. Acta*, 2020, 268, 405–421. https://doi.org/10.1016/j.gca.2019.10.017.
58. W. Russell and D. Papanastassiou, Calcium Isotope Fractionation in Ion-Exchange Chromatography, *Anal. Chem.*, 1978, 50 (8), 1151–1154. https://doi.org/10.1021/ac50030a036
59. V. Balter and C. Lécuyer, Determination of Sr and Ba Partition Coefficients between Apatite and Water from 5 C to 60 C: a Potential New Thermometer for Aquatic Paleoenvironments, *Geochim. Cosmochim. Acta*, 2004, 68 (3), 423–432. https://doi.org/10.1016/S0016-7037(03)00453-8.
60. V. Balter and C. Lécuyer, Determination of Sr and Ba Partition Coefficients between Apatite from Fish (*Sparusaurata*) and

Seawater: the influence of Temperature, *Geochim. Cosmochim. Acta*, 2010, 74 (12), 3449–3458. https://doi.org/10.1016/j.gca.2010.03.015.
61. D. Bevan, C. D. Coath, J. Lewis, J. Schwieters, N. Lloyd, G. Craig, H. Wehrs and T. Elliott, *In situ* Rb-Sr Dating by Collision Cell, Multicollection Inductively-Coupled Plasma Mass-Spectrometry with Pre-Cell Mass-Filter, (CC-MC-ICPMS/MS), *J. Anal. At. Spectrom.*, 2021, 36 (5), 917–931. https://doi.org/10.1039/D1JA00006C.
62. G. C. Eiden, C. J. Barinaga and D. W. Koppenaal, Selective Removal of Plasma Matrix Ions in Plasma Source Mass Spectrometry, *J. Anal. At. Spectrom.*, 1996, 11 (4), 317–322. https://doi.org/10.1039/ja9961100317.
63. J. Lewis, T. -. H. Luu, C. D. Coath, H. Wehrs, J. B. Schwieters and T. Elliott, Collision Course; High-Precision Mass-Independent and Mass-Dependent Calcium Isotope Measurements Using the Prototype Collision Cell MC-ICPMS/MS, Proteus, *Chem. Geol.*, 2022, 614, 121185. https://doi.org/10.1016/j.chemgeo.2022.121185.
64. S. Weyer and J. Schwieters, High Precision Fe Isotope Measurements with High Mass Resolution MC-ICPMS, *Int. J. Mass Spectrom.*, 2003, 226 (3), 355–368. https://doi.org/10.1016/S1387-3806(03)00078-2.
65. F. Albarède and B. Beard, Analytical Methods for Non-Traditional Isotopes, *Rev. Mineral. Geochem.*, 2004, 55 (1), 113–152. https://doi.org/10.2138/gsrmg.55.1.113.
66. J. Lewis, T. H. Luu, C. D. Coath, H. Wehrs, T. Elliott and J. B. Schwieters, Collision Course: Accurate and Precise Measurements of Stable and Radiogenic Calcium Isotopes Using the Collision Cell MC-ICPMS, Proteus, *AGU Fall Meeting Abstracts*. 2018, V43A–V403
67. R. C. Hin, C. D. Coath, J. Carter philip, F. Nimmo, Y. -. J. Lai, P. A. E. Pogge von Strandmann, M. Willbold, Z. M. Leinhardt, J. Walter michael and T. Elliott, Magnesium Isotope Evidence that Accretional Vapour Loss Shapes Planetary Compositions, *Nature*, 2017, 549 (7673), 511–515. https://doi.org/10.1038/nature23899
68. M. Lok, *The IUPAC Compendium of Chemical Terminology*. V Gold (ed.). Research Triangle Park, NC: International Union of Pure and Applied Chemistry (IUPAC), 2019.
69. H. Chen, Z. Tian, B. Tuller-Ross, R. L. Korotev and K. Wang, High-Precision Potassium Isotopic Analysis by MC-ICP-MS: an Inter-Laboratory Comparison and Refined K Atomic Weight, *J. Anal. At. Spectrom.*, 2019, 34 (1), 160–171.
70. Y.-K. Xu, Y. Hu, X.-Y. Chen, T.-Y. Huang, R. S. Sletten, D. Zhu and F.-Z. Teng, Potassium Isotopic Compositions of International Geological Reference Materials, *Chem. Geol.*, 2019, 513, 101–107. https://doi.org/10.1016/j.chemgeo.2019.03.010.
71. P. Télouk, E. Albalat, T. Tacail, F. Arnaud-Godet and V. Balter, Steady Analyses of Potassium Stable Isotopes Using a Thermo Scientific Neoma MC-ICP-MS, *J. Anal. At. Spectrom.*, 2022, 37 (6), 1259–1264. https://doi.org/10.1039/D2JA00050D.
72. R Core Team, *R: a Language and Environment for Statistical Computing*, R Found Stat Comput Vienna, Austria 2016.
73. K. Jaouen, L. Pouilloux, V. Balter, M.-L. Pons, J.-J. Hublin and F. Albarède, Dynamic Homeostasis Modeling of Zn Isotope Ratios in the Human Body, *Metallomics*, 2019, 11 (6), 1049–1059. https://doi.org/10.1039/c8mt00286j.
74. A. Hassler, J. E. Martin, S. Ferchaud, D. Grivault, S. Le Goff, E. Albalat, J. -. A. Hernandez, T. Tacail and V. Balter, Lactation and Gestation Controls on Calcium Isotopic Compositions in a Mammalian Model, *Metallomics*, 2021, 13 (6), 1–15. https://doi.org/10.1093/mtomcs/mfab019.
75. T. Tacail, isobxr: Stable Isotope Box Modelling in R, 2021. https://cran.r-project.org/web/packages/isobxr/index.html.
76. T. B. Coplen, Guidelines and Recommended Terms for Expression of Stable-Isotope-Ratio and Gas-Ratio Measurement Results, *Rapid Comm. Mass Spectrom.*, 2011, 25 (17), 2538–2560. https://doi.org/10.1002/rcm.5129.
77. F. Albarède, P. Télouk and V. Balter, Medical applications of isotope metallomics, *Rev. Mineral. Geochem.*, 2017, 82 (1), 851–885. https://doi.org/10.2138/rmg.2017.82.20.
78. F. Moynier, T. Fujii, A. S. Shaw and M. Le Borgne, Heterogeneous Distribution of Natural Zinc Isotopes in Mice, *Metallomics*, 2013, 5 (6), 693–699. https://doi.org/10.1039/c3mt00008g
79. L. A. Kadir, M. Stacey and R. Barrett-Jolley, Emerging Roles of the Membrane Potential: Action Beyond the Action Potential, *Front. Physiol.*, 2018, 9, 1–10.
80. L. F. Santana, E. P. Cheng and W. J. Lederer, How Does the Shape of the Cardiac Action Potential Control Calcium Signaling and Contraction in the Heart?*J. Mol. Cell Cardiol.*, 2010, 49 (6), 901–903. https://doi.org/10.1016/j.yjmcc.2010.09.005
81. J. Graf and O. H. Petersen, Cell Membrane Potential and Resistance in Liver, *J. Physiol.*, 1978, 284 (1), 105–126. https://doi.org/10.1113/jphysiol.1978.sp012530.
82. M. M. Balach, C. H. Casale and A. N. Campetelli, Erythrocyte Plasma Membrane Potential: Past and Current Methods for Its Measurement, *Biophys. Rev.*, 2019, 11 (6), 995–1005. https://doi.org/10.1007/s12551-019-00603-5.
83. R. Qu and G. Han, Potassium Isotopes in Herbaceous Plants: a Potential New Tool for C 3 and C 4 Plant Research, *JGR Biogeosci.*, 2022, 127 (11), https://doi.org/10.1029/2021JG006682.
84. T. Shinoda, H. Ogawa, F. Cornelius and C. Toyoshima, Crystal Structure of the Sodium-Potassium Pump at 2.4 Resolution, *Nature*, 2009, 459 (7245), 446–450. https://doi.org/10.1038/nature07939
85. J. P. Castillo, H. Rui, D. Basilio, A. Das, B. Roux, R. Latorre, F. Bezanilla and M. Holmgren, Mechanism of Potassium Ion Uptake by the Na+/K+-ATPase, *Nat. Commun.*, 2015, 6 (1), 7622. https://doi.org/10.1038/ncomms8622.
86. M. I. Lindinger and S. P. Cairns, Regulation of Muscle Potassium: Exercise Performance, Fatigue and Health Implications, *Eur. J. Appl. Physiol.*, 2021, 121 (3), 721–748. https://doi.org/10.1007/s00421-020-04546-8.
87. Q. Kuang, P. Purhonen and H. Hebert, Structure of Potassium Channels, *Cell. Mol. Life Sci.*, 2015, 72 (19), 3677–3693. https://doi.org/10.1007/s00018-015-1948-5.
88. S. Durdagi, B. Roux and S. Y. Noskov, Potassium-Binding Site Types in Proteins, *Encyclopedia of Metalloproteins*. New York, NY: Springer, 2013, 1809–1815.
89. H. R. Pohl, J. S. Wheeler and H. E. Murray, Sodium and Potassium in Health and Disease, In: Sigel, A., Sigel, H., Sigel, R. (eds.), *Interrelations between Essential Metal Ions and Human Diseases*. Metal Ions in Life Sciences, Vol. 13. Dordrecht: Springer. https://doi.org/10.1007/978-94-007-7500-8_2.
90. F. Moynier and T. Fujii, Calcium Isotope Fractionation between Aqueous Compounds Relevant to Low-Temperature Geochemistry, Biology and Medicine, *Sci. Rep.*, 2017, 7 (1), 44255. https://doi.org/10.1038/srep44255.
91. G. V. Iyengar, W. E. Kollmer and H. J. M. Bowen, *The Elemental Composition of Human Tissues and Body Fluids*. Weinheim: Verlag Chemie, 1978.
92. K. Bremner, W. A. Bubb, G. J. Kemp, M. I. Trenell and C. H. Thompson, The Effect of Phosphate Loading on Erythrocyte 2,3-Bisphosphoglycerate Levels, *Clin. Chim. Acta*, 2002, 323 (1-2), 111–114. https://doi.org/10.1016/S0009-8981(02)00165-1
93. J. P. Knochel, R. Haller and E. Ferguson, Selective Phosphorus Deficiency in the Hyperalimented Hypophosphatemic Dog and Phosphorylation Potentials in the Muscle Cell, In: S.G.

Massry, E. Ritz and H. Jahn (eds.), *Phosphate and Minerals in Health and Disease*. Advances in Experimental Medicine and Biology, 1980, 128. Boston, MA: Springer. https://doi.org/10.1007/978-1-4615-9167-2_37

94. D. Shier, J. Butler and R. Lewis, *Hole's Human Anatomy & Physiology*. 14th Edn. New York: McGraw-Hill Education, 2016.
95. M. Yang and W. J. Brackenbury, Membrane Potential and Cancer Progression, *Front. Physiol.*, 2013, 4, 1–10. https://doi.org/10.3389/fphys.2013.00185.
96. S. Truchet and E. Honvo-Houéto, Physiology of Milk Secretion, *Best Pract. Res. Clin. Endocrinol. Metab.*, 2017, 31 (4), 367–384. https://doi.org/10.1016/j.beem.2017.10.008.
97. D. B. Shennan and M. Peaker, Transport of Milk Constituents by the Mammary Gland, *Physiol. Rev.*, 2000, 80 (3), 925–951. https://doi.org/10.1152/physrev.2000.80.3.925.
98. J. M. Williams, C. A. Duckworth, M. D. Burkitt, A. J. M. Watson, B. J. Campbell and D. M. Pritchard, Epithelial Cell Shedding and Barrier Function: a Matter of Life and Death at the Small Intestinal Villus Tip, *Vet. Pathol.*, 2015, 52 (3), 445–455. https://doi.org/10.1177/0300985814559404.
99. V. M. Rajendran and G. I. Sandle, Colonic Potassium Absorption and Secretion in Health and Disease, *Compr. Physiol.*, 2018, 8, 1513–1536. https://doi.org/10.1002/cphy.c170030.
100. S. Yamada and M. Inaba, Potassium Metabolism and Management in Patients with CKD, *Nutrients*, 2021, 13 (6), 1–19. https://doi.org/10.3390/nu13061751.
101. M. V. Clausen, F. Hilbers and H. Poulsen, The Structure and Function of the Na,K-ATPase Isoforms in Health and Disease, *Front. Physiol.*, 2017, 8, 1–16. https://doi.org/10.3389/fphys.2017.00371